

日本原子力研究開発機構機関リポジトリ  
Japan Atomic Energy Agency Institutional Repository

Title	Amplitude analysis of $e^+e^- \rightarrow \mathcal{T}(nS) \pi^+\pi^-$ at $\sqrt{s}=10.866$ GeV
Author(s)	Garmash A., Tanida Kiyoshi, Belle Collaboration
Citation	Physical Review D, 91(7), 072003(2015)
Text Version	Publisher
URL	<a href="http://jolissrch-inter.tokai-sc.jaea.go.jp/search/servlet/search?5053218">http://jolissrch-inter.tokai-sc.jaea.go.jp/search/servlet/search?5053218</a>
DOI	<a href="http://dx.doi.org/10.1103/PhysRevD.91.072003">http://dx.doi.org/10.1103/PhysRevD.91.072003</a>
Right	©2015 The American Physical Society

**Amplitude analysis of  $e^+e^- \rightarrow \Upsilon(nS)\pi^+\pi^-$  at  $\sqrt{s} = 10.866$  GeV**

A. Garmash,<sup>4</sup> A. Bondar,<sup>4</sup> A. Kuzmin,<sup>4</sup> A. Abdesselam,<sup>55</sup> I. Adachi,<sup>13</sup> H. Aihara,<sup>60</sup> S. Al Said,<sup>55,69</sup> D. M. Asner,<sup>47</sup> V. Aulchenko,<sup>4</sup> T. Aushev,<sup>21</sup> R. Ayad,<sup>55</sup> A. M. Bakich,<sup>54</sup> A. Bala,<sup>48</sup> V. Bhardwaj,<sup>38</sup> A. Bobrov,<sup>4</sup> G. Bonvicini,<sup>66</sup> A. Bozek,<sup>42</sup> M. Bračko,<sup>32,22</sup> T. E. Browder,<sup>12</sup> D. Červenkov,<sup>5</sup> V. Chekelian,<sup>33</sup> A. Chen,<sup>39</sup> B. G. Cheon,<sup>11</sup> K. Chilikin,<sup>21</sup> R. Chistov,<sup>21</sup> K. Cho,<sup>26</sup> V. Chobanova,<sup>33</sup> Y. Choi,<sup>53</sup> D. Cinabro,<sup>66</sup> J. Dalseno,<sup>33,57</sup> Z. Doležal,<sup>5</sup> A. Drutskoy,<sup>21,35</sup> D. Dutta,<sup>15</sup> S. Eidelman,<sup>4</sup> D. Epifanov,<sup>60</sup> H. Farhat,<sup>66</sup> J. E. Fast,<sup>47</sup> T. Ferber,<sup>8</sup> A. Frey,<sup>10</sup> O. Frost,<sup>8</sup> V. Gaur,<sup>56</sup> S. Ganguly,<sup>66</sup> R. Gillard,<sup>66</sup> R. Glattauer,<sup>18</sup> Y. M. Goh,<sup>11</sup> B. Golob,<sup>30,22</sup> J. Haba,<sup>13</sup> T. Hara,<sup>13</sup> K. Hayasaka,<sup>37</sup> H. Hayashii,<sup>38</sup> X. H. He,<sup>49</sup> Y. Hoshi,<sup>58</sup> W.-S. Hou,<sup>41</sup> Y. B. Hsiung,<sup>41</sup> H. J. Hyun,<sup>28</sup> T. Iijima,<sup>37,36</sup> A. Ishikawa,<sup>59</sup> R. Itoh,<sup>13</sup> Y. Iwasaki,<sup>13</sup> T. Iwashita,<sup>25</sup> I. Jaegle,<sup>12</sup> T. Julius,<sup>34</sup> J. H. Kang,<sup>68</sup> E. Kato,<sup>59</sup> P. Katrenko,<sup>21</sup> H. Kawai,<sup>6</sup> T. Kawasaki,<sup>44</sup> H. Kichimi,<sup>13</sup> C. Kiesling,<sup>33</sup> D. Y. Kim,<sup>52</sup> J. B. Kim,<sup>27</sup> J. H. Kim,<sup>26</sup> K. T. Kim,<sup>27</sup> M. J. Kim,<sup>28</sup> Y. J. Kim,<sup>26</sup> K. Kinoshita,<sup>7</sup> J. Klucar,<sup>22</sup> B. R. Ko,<sup>27</sup> P. Kodyš,<sup>5</sup> S. Korpar,<sup>32,22</sup> P. Križan,<sup>30,22</sup> P. Krokovny,<sup>4</sup> T. Kuhr,<sup>24</sup> Y.-J. Kwon,<sup>68</sup> S.-H. Lee,<sup>27</sup> Y. Li,<sup>65</sup> L. Li Gioi,<sup>33</sup> J. Libby,<sup>16</sup> C. Liu,<sup>50</sup> Z. Q. Liu,<sup>17</sup> D. Liventsev,<sup>13</sup> P. Lukin,<sup>4</sup> D. Matvienko,<sup>4</sup> K. Miyabayashi,<sup>38</sup> H. Miyata,<sup>44</sup> R. Mizuk,<sup>21,35</sup> G. B. Mohanty,<sup>56</sup> A. Moll,<sup>33,57</sup> R. Mussa,<sup>20</sup> E. Nakano,<sup>46</sup> M. Nakao,<sup>13</sup> Z. Natkaniec,<sup>42</sup> M. Nayak,<sup>16</sup> E. Nedelkovska,<sup>33</sup> N. K. Nisar,<sup>56</sup> S. Nishida,<sup>13</sup> O. Nitoh,<sup>63</sup> S. Okuno,<sup>23</sup> S. L. Olsen,<sup>51</sup> W. Ostrowicz,<sup>42</sup> P. Pakhlov,<sup>21,35</sup> H. Park,<sup>28</sup> H. K. Park,<sup>28</sup> T. K. Pedlar,<sup>31</sup> R. Pestotnik,<sup>22</sup> M. Petrič,<sup>22</sup> L. E. Pilonen,<sup>65</sup> E. RIBEŽIČ,<sup>22</sup> M. Ritter,<sup>33</sup> M. Röhrken,<sup>24</sup> A. Rostomyan,<sup>8</sup> S. Ryu,<sup>51</sup> T. Saito,<sup>59</sup> Y. Sakai,<sup>13</sup> S. Sandilya,<sup>56</sup> D. Santel,<sup>7</sup> T. Sanuki,<sup>59</sup> Y. Sato,<sup>59</sup> O. Schneider,<sup>29</sup> G. Schnell,<sup>1,14</sup> A. J. Schwartz,<sup>7</sup> D. Semmler,<sup>9</sup> K. Senyo,<sup>67</sup> M. E. Seviar,<sup>34</sup> M. Shapkin,<sup>19</sup> V. Shebalin,<sup>4</sup> C. P. Shen,<sup>2</sup> T.-A. Shibata,<sup>61</sup> J.-G. Shiu,<sup>41</sup> B. Shwartz,<sup>4</sup> F. Simon,<sup>33,57</sup> Y.-S. Sohn,<sup>68</sup> A. Sokolov,<sup>19</sup> E. Solovieva,<sup>21</sup> S. Stanič,<sup>45</sup> M. Starič,<sup>22</sup> M. Steder,<sup>8</sup> T. Sumiyoshi,<sup>62</sup> U. Tamponi,<sup>20,64</sup> K. Tanida,<sup>51</sup> G. Tatishvili,<sup>47</sup> Y. Teramoto,<sup>46</sup> K. Trabelsi,<sup>13</sup> M. Uchida,<sup>61</sup> Y. Unno,<sup>11</sup> S. Uno,<sup>13</sup> P. Urquijo,<sup>3</sup> Y. Usov,<sup>4</sup> C. Van Hulse,<sup>1</sup> P. Vanhoefer,<sup>33</sup> G. Varner,<sup>12</sup> A. Vinokurova,<sup>4</sup> V. Vorobyev,<sup>4</sup> M. N. Wagner,<sup>9</sup> C. H. Wang,<sup>40</sup> P. Wang,<sup>17</sup> X. L. Wang,<sup>65</sup> M. Watanabe,<sup>44</sup> Y. Watanabe,<sup>23</sup> K. M. Williams,<sup>65</sup> E. Won,<sup>27</sup> H. Yamamoto,<sup>59</sup> Y. Yamashita,<sup>43</sup> S. Yashchenko,<sup>8</sup> Y. Yook,<sup>68</sup> C. Z. Yuan,<sup>17</sup> Z. P. Zhang,<sup>50</sup> V. Zhilich,<sup>4</sup> and A. Zupanc<sup>22</sup>

(Belle Collaboration)

<sup>1</sup>University of the Basque Country UPV/EHU, 48080 Bilbao<sup>2</sup>Beihang University, Beijing 100191<sup>3</sup>University of Bonn, 53115 Bonn<sup>4</sup>Budker Institute of Nuclear Physics SB RAS and Novosibirsk State University, Novosibirsk 630090<sup>5</sup>Faculty of Mathematics and Physics, Charles University, 121 16 Prague<sup>6</sup>Chiba University, Chiba 263-8522<sup>7</sup>University of Cincinnati, Cincinnati, Ohio 45221<sup>8</sup>Deutsches Elektronen-Synchrotron, 22607 Hamburg<sup>9</sup>Justus-Liebig-Universität Gießen, 35392 Gießen<sup>10</sup>II. Physikalisches Institut, Georg-August-Universität Göttingen, 37073 Göttingen<sup>11</sup>Hanyang University, Seoul 133-791<sup>12</sup>University of Hawaii, Honolulu, Hawaii 96822<sup>13</sup>High Energy Accelerator Research Organization (KEK), Tsukuba 305-0801<sup>14</sup>IKERBASQUE, Basque Foundation for Science, 48011 Bilbao<sup>15</sup>Indian Institute of Technology Guwahati, Assam 781039<sup>16</sup>Indian Institute of Technology Madras, Chennai 600036<sup>17</sup>Institute of High Energy Physics, Chinese Academy of Sciences, Beijing 100049<sup>18</sup>Institute of High Energy Physics, Vienna 1050<sup>19</sup>Institute for High Energy Physics, Protvino 142281<sup>20</sup>INFN-Sezione di Torino, 10125 Torino<sup>21</sup>Institute for Theoretical and Experimental Physics, Moscow 117218<sup>22</sup>J. Stefan Institute, 1000 Ljubljana<sup>23</sup>Kanagawa University, Yokohama 221-8686<sup>24</sup>Institut für Experimentelle Kernphysik, Karlsruher Institut für Technologie, 76131 Karlsruhe<sup>25</sup>Kavli Institute for the Physics and Mathematics of the Universe (WPI),

University of Tokyo, Kashiwa 277-8583

<sup>26</sup>Korea Institute of Science and Technology Information, Daejeon 305-806<sup>27</sup>Korea University, Seoul 136-713<sup>28</sup>Kyungpook National University, Daegu 702-701<sup>29</sup>École Polytechnique Fédérale de Lausanne (EPFL), Lausanne 1015<sup>30</sup>Faculty of Mathematics and Physics, University of Ljubljana, 1000 Ljubljana<sup>31</sup>Luther College, Decorah, Iowa 52101<sup>32</sup>University of Maribor, 2000 Maribor

- <sup>33</sup>Max-Planck-Institut für Physik, 80805 München  
<sup>34</sup>School of Physics, University of Melbourne, Victoria 3010  
<sup>35</sup>Moscow Physical Engineering Institute, Moscow 115409  
<sup>36</sup>Graduate School of Science, Nagoya University, Nagoya 464-8602  
<sup>37</sup>Kobayashi-Maskawa Institute, Nagoya University, Nagoya 464-8602  
<sup>38</sup>Nara Women's University, Nara 630-8506  
<sup>39</sup>National Central University, Chung-li 32054  
<sup>40</sup>National United University, Miao Li 36003  
<sup>41</sup>Department of Physics, National Taiwan University, Taipei 10617  
<sup>42</sup>H. Niewodniczanski Institute of Nuclear Physics, Krakow 31-342  
<sup>43</sup>Nippon Dental University, Niigata 951-8580  
<sup>44</sup>Niigata University, Niigata 950-2181  
<sup>45</sup>University of Nova Gorica, 5000 Nova Gorica  
<sup>46</sup>Osaka City University, Osaka 558-8585  
<sup>47</sup>Pacific Northwest National Laboratory, Richland, Washington 99352  
<sup>48</sup>Panjab University, Chandigarh 160014  
<sup>49</sup>Peking University, Beijing 100871  
<sup>50</sup>University of Science and Technology of China, Hefei 230026  
<sup>51</sup>Seoul National University, Seoul 151-742  
<sup>52</sup>Soongsil University, Seoul 156-743  
<sup>53</sup>Sungkyunkwan University, Suwon 440-746  
<sup>54</sup>School of Physics, University of Sydney, NSW 2006  
<sup>55</sup>Department of Physics, Faculty of Science, University of Tabuk, Tabuk 71451  
<sup>56</sup>Tata Institute of Fundamental Research, Mumbai 400005  
<sup>57</sup>Excellence Cluster Universe, Technische Universität München, 85748 Garching  
<sup>58</sup>Tohoku Gakuin University, Tagajo 985-8537  
<sup>59</sup>Tohoku University, Sendai 980-8578  
<sup>60</sup>Department of Physics, University of Tokyo, Tokyo 113-0033  
<sup>61</sup>Tokyo Institute of Technology, Tokyo 152-8550  
<sup>62</sup>Tokyo Metropolitan University, Tokyo 192-0397  
<sup>63</sup>Tokyo University of Agriculture and Technology, Tokyo 184-8588  
<sup>64</sup>University of Torino, 10124 Torino  
<sup>65</sup>CNP, Virginia Polytechnic Institute and State University, Blacksburg, Virginia 24061  
<sup>66</sup>Wayne State University, Detroit, Michigan 48202  
<sup>67</sup>Yamagata University, Yamagata 990-8560  
<sup>68</sup>Yonsei University, Seoul 120-749  
<sup>69</sup>Department of Physics, Faculty of Science, King Abdulaziz University, Jeddah 21589  
(Received 7 March 2014; published 6 April 2015)

We report results on studies of the  $e^+e^-$  annihilation into three-body  $\Upsilon(nS)\pi^+\pi^-$  ( $n = 1, 2, 3$ ) final states including measurements of cross sections and the full amplitude analysis. The cross sections measured at  $\sqrt{s} = 10.866$  GeV and corrected for the initial state radiation are  $\sigma(e^+e^- \rightarrow \Upsilon(1S)\pi^+\pi^-) = (2.27 \pm 0.12 \pm 0.14)$  pb,  $\sigma(e^+e^- \rightarrow \Upsilon(2S)\pi^+\pi^-) = (4.07 \pm 0.16 \pm 0.45)$  pb, and  $\sigma(e^+e^- \rightarrow \Upsilon(3S)\pi^+\pi^-) = (1.46 \pm 0.09 \pm 0.16)$  pb. Amplitude analysis of the three-body  $\Upsilon(nS)\pi^+\pi^-$  final states strongly favors  $I^G(J^P) = 1^+(1^+)$  quantum-number assignments for the two bottomonium-like  $Z_b^\pm$  states, recently observed in the  $\Upsilon(nS)\pi^\pm$  and  $h_b(mP)\pi^\pm$  ( $m = 1, 2$ ) decay channels. The results are obtained with a  $121.4 \text{ fb}^{-1}$  data sample collected with the Belle detector at the KEKB asymmetric-energy  $e^+e^-$  collider.

DOI: 10.1103/PhysRevD.91.072003

PACS numbers: 14.40.Pq, 12.39.Pn, 13.25.Gv

## I. INTRODUCTION

Analysis of the  $\Upsilon(10860)$  decays to non- $B\bar{B}$  final states has led to several surprises. Recently, the Belle Collaboration reported observation of anomalously high rates for the  $e^+e^- \rightarrow \Upsilon(nS)\pi^+\pi^-$  ( $n = 1, 2, 3$ ) [1] and  $e^+e^- \rightarrow h_b(mP)\pi^+\pi^-$  ( $m = 1, 2$ ) [2] transitions measured in the vicinity of the  $\Upsilon(10860)$  peak. If the  $\Upsilon(nS)$  signals

are attributed entirely to the  $\Upsilon(10860)$  decays, the measured partial decay widths  $\Gamma[\Upsilon(10860) \rightarrow \Upsilon(nS)\pi^+\pi^-] \sim 0.5$  MeV are about 2 orders of magnitude larger than the typical widths for the dipion transitions amongst  $\Upsilon(nS)$  states with  $n \leq 4$ . In addition, the rates of the  $e^+e^- \rightarrow h_b(mP)\pi^+\pi^-$  processes are found to be comparable with those for  $e^+e^- \rightarrow \Upsilon(nS)\pi^+\pi^-$ , and hence the process with a spin flip of the heavy quark [that is,  $h_b(mP)$  production]

is not suppressed. These unexpected observations indicate that an exotic mechanism might contribute to the  $\Upsilon(10860)$  decays. A detailed analysis of the three-body  $e^+e^- \rightarrow \Upsilon(nS)\pi^+\pi^-$  and  $e^+e^- \rightarrow h_b(mP)\pi^+\pi^-$  processes reported by Belle [3] revealed the presence of two charged bottomonium-like states, denoted as  $Z_b(10610)^\pm$  and  $Z_b(10650)^\pm$ . These two resonances are observed in the decay chains  $e^+e^- \rightarrow Z_b^\pm \pi^\mp \rightarrow \Upsilon(nS)\pi^+\pi^-$  and  $e^+e^- \rightarrow Z_b^\pm \pi^\mp \rightarrow h_b(mP)\pi^+\pi^-$ . The nonresonant contribution is found to be sizable in the  $\Upsilon(nS)\pi^+\pi^-$  channels and consistent with zero in the  $h_b(mP)\pi^+\pi^-$  ones. Masses and widths of the  $Z_b^\pm$  states have been measured in a (one-) two-dimensional amplitude analysis of the three-body ( $e^+e^- \rightarrow h_b(mP)\pi^+\pi^-$ )  $e^+e^- \rightarrow \Upsilon(nS)\pi^+\pi^-$  transitions [3]. Also, observation of the neutral  $Z_b(10610)^0$  partner has been reported recently by Belle [4]. Although the simplified angular analysis in Ref. [5] favors the  $J^P = 1^+$  assignment for the two charged  $Z_b$  states, the discrimination power against other possible combinations is not high enough to claim this assignment unequivocally.

Results of the analysis of three-body  $e^+e^- \rightarrow \Upsilon(nS)\pi^+\pi^-$  processes presented in this paper are obtained by utilizing full amplitude analysis in six-dimensional phase space that not only allow us to determine the relative fractions of intermediate components but also provide high sensitivity to the spin and parity of the  $Z_b$  states. Results on the  $e^+e^-$  annihilation to the three-body  $\Upsilon(nS)\pi^+\pi^-$  final states reported here supersede those published in Ref. [1].

We use a data sample with an integrated luminosity of  $121.4 \text{ fb}^{-1}$  collected at the peak of the  $\Upsilon(10860)$  resonance ( $\sqrt{s} = 10.866 \text{ GeV}$ ) with the Belle detector at the KEKB asymmetric-energy  $e^+e^-$  collider [6].

## II. BELLE DETECTOR

The Belle detector [7] is a large-solid-angle magnetic spectrometer based on a 1.5 T superconducting solenoid magnet. Charged particle tracking is provided by a four-layer silicon vertex detector and a 50-layer central drift chamber (CDC) that surround the interaction point. The charged particle acceptance covers laboratory polar angles between  $\theta = 17^\circ$  and  $150^\circ$ , corresponding to about 92% of the total solid angle in the center-of-mass (c.m.) frame.

Charged hadron identification is provided by  $dE/dx$  measurements in the CDC, an array of 1188 aerogel Cherenkov counters (ACC), and a barrel-like array of 128 time-of-flight scintillation counters (TOF); information from the three subdetectors is combined to form likelihood ratios, which are then used for pion, kaon and proton discrimination. Electromagnetic showering particles are detected in an array of 8736 CsI(Tl) crystals (ECL) that covers the same solid angle as the charged particle tracking system. Electron identification in Belle is based on a combination of  $dE/dx$  measurements in the CDC, the response of the ACC, and the position, shape and total

energy deposition (i.e.,  $E/p$ ) of the shower detected in the ECL. The electron identification efficiency is greater than 92% for tracks with  $p_{\text{lab}} > 1.0 \text{ GeV}/c$ , and the hadron misidentification probability is below 0.3%. The magnetic field is returned via an iron yoke that is instrumented to detect muons and  $K_L^0$  mesons. Muons are identified based on their penetration range and transverse scattering in the KLM detector. In the momentum region relevant to this analysis, the identification efficiency is about 90% while the probability to misidentify a pion as a muon is below 2%.

We use the EvtGen event generator [8] with PHOTOS [9] for radiative corrections and a GEANT-based Monte Carlo (MC) simulation [10] to model the response of the detector and determine the acceptance. The MC simulation includes run-dependent detector performance variations and background conditions.

## III. EVENT SELECTION

Charged tracks are selected with a set of track quality requirements based on the average hit residual and on the distances of closest approach to the interaction point. We require four well-reconstructed tracks with a net zero charge in the event, with two of them, oppositely charged, identified as muons and the other two consistent with pions. We also require that none of the four tracks be identified as an electron (electron veto).

Candidate  $e^+e^- \rightarrow \Upsilon(nS)\pi^+\pi^- \rightarrow \mu^+\mu^-\pi^+\pi^-$  events are identified via the measured invariant mass of the  $\mu^+\mu^-$  combination and the recoil mass,  $M_{\text{miss}}(\pi^+\pi^-)$ , associated with the  $\pi^+\pi^-$  system, defined by

$$M_{\text{miss}}(\pi^+\pi^-) = \sqrt{(E_{\text{c.m.}} - E_{\pi\pi}^*)^2 - p_{\pi\pi}^{*2}}, \quad (1)$$

where  $E_{\text{c.m.}}$  is the c.m. energy and  $E_{\pi\pi}^*$  and  $p_{\pi\pi}^*$  are the energy and momentum of the  $\pi^+\pi^-$  system measured in the c.m. frame. The two-dimensional distribution of  $M(\mu^+\mu^-)$  versus  $M_{\text{miss}}(\pi^+\pi^-)$  for all selected candidates is shown in Fig. 1. Events originating from the  $e^+e^- \rightarrow \mu^+\mu^-\pi^+\pi^-$  process fall within a narrow diagonal band (signal region) that is defined as  $|M_{\text{miss}}(\pi^+\pi^-) - M(\mu^+\mu^-)| < 0.2 \text{ GeV}/c^2$  (see Fig. 1). Concentrations of events within the signal region near the  $\Upsilon(nS)$  nominal masses are apparent on the plot. Clusters of events below the diagonal band are mainly due to initial state radiation (ISR)  $e^+e^- \rightarrow \Upsilon(2S, 3S)\gamma$  processes and inclusive  $e^+e^- \rightarrow \Upsilon(2S, 3S)X$  ( $X = \pi^+\pi^-, \eta$ , etc.) production with a subsequent dipion transition of the  $\Upsilon(2S, 3S)$  state to the ground  $\Upsilon(1S)$  state. The one-dimensional  $M_{\text{miss}}(\pi^+\pi^-)$  projections for events in the signal region are shown in Fig. 2, where an additional requirement on the invariant mass of the  $\pi^+\pi^-$  system,  $M(\pi^+\pi^-)$ , is imposed (see Table I) to suppress the background from photon conversion in the inner parts of the Belle detector. We perform a binned maximum likelihood

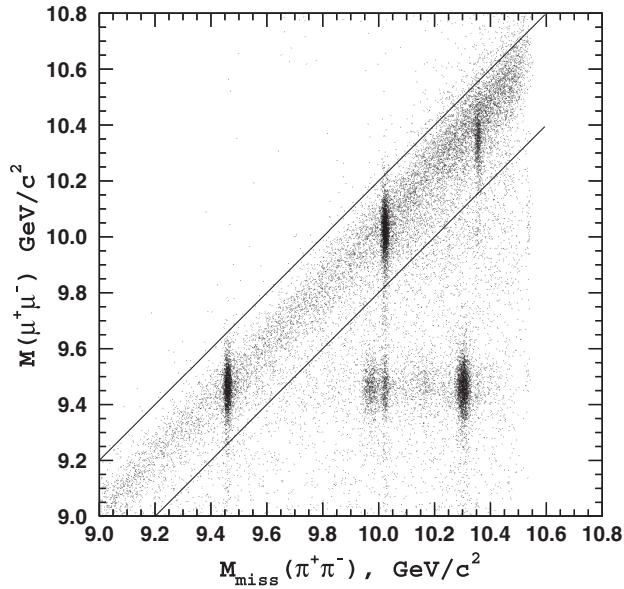


FIG. 1. Scatter plot of all the  $e^+e^- \rightarrow \Upsilon(nS)\pi^+\pi^-$  candidate events passed through initial selection criteria. The region between the two diagonal lines is defined as the signal region.

fit to the  $M_{\text{miss}}(\pi^+\pi^-)$  distributions with a sum of a Crystal Ball function [11] for the  $\Upsilon(nS)$  signal and a linear function for the combinatorial background component. The Crystal Ball function is used to account for the asymmetric shape of the  $\Upsilon(nS)$  signal due to initial state radiation of soft photons. All parameters (seven in total) are free parameters of the fit. Results of the fits are shown in Fig. 2 and summarized in Table I.

For the subsequent analysis, we select events around the respective  $\Upsilon(nS)$  mass peak as specified in Table I. After all the selections are applied, we are left with 1905, 2312, and 635 candidate events for the  $\Upsilon(1S)\pi^+\pi^-$ ,  $\Upsilon(2S)\pi^+\pi^-$ , and  $\Upsilon(3S)\pi^+\pi^-$  final state, respectively. The fractions of signal events in the selected samples are determined using results of the fit to the corresponding  $M_{\text{miss}}(\pi^+\pi^-)$  spectrum (see Table I). For selected events, we perform a mass-constrained fit of the  $\mu^+\mu^-$  pair to the nominal mass of the

corresponding  $\Upsilon(nS)$  state to improve the  $\Upsilon(nS)\pi$  invariant mass resolution.

#### IV. AMPLITUDE ANALYSIS

In the limit of negligible  $\Upsilon(nS)$  width, the process  $e^+e^- \rightarrow \Upsilon(nS)\pi^+\pi^- \rightarrow \mu^+\mu^-$  is described by six independent parameters. A set of physics observables is not unique and, in particular, depends on whether there is a resonant state in the  $\pi^+\pi^-$  or in the  $\Upsilon(nS)\pi$  system. As an example, a convenient set of observables for the process  $e^+e^- \rightarrow Z_b^+\pi^- \rightarrow \Upsilon(nS)\pi^+\pi^-$  is the following: masses  $M(\Upsilon(nS)\pi^+)$  and  $M(\pi^+\pi^-)$ , the angle between the prompt pion and the beam axis in the c.m. frame ( $\theta_1$ ), the angle between the  $Z_b^+$  and the  $\mu^+$  momenta calculated in the  $\Upsilon(nS)$  rest frame [that is, the  $\Upsilon(nS) \rightarrow \mu^+\mu^-$  helicity angle,  $\theta_{\mu\mu}^{\text{hel}}$ ], the angle between the plane formed by the  $\pi^+\pi^-$  system and the  $\Upsilon(nS)$  decay plane in the  $Z_b$  rest frame ( $\phi$ ), and, finally, the angle between the plane formed by the prompt pion and the beam axis and the  $\Upsilon(nS)$  decay plane calculated in the  $Z_b$  rest frame ( $\psi$ ). However, this set of observables is not convenient to parametrize amplitudes with a resonant state in the  $\pi^+\pi^-$  system [such as  $e^+e^- \rightarrow \Upsilon(nS)f_0(980)$ ]; thus, we use these parameters only for visualization of fit results. The transition amplitude is written in Lorentz-invariant form as discussed in detail in the Appendix. The six parameters in this case are invariant masses of six independent two-particle combinations composed of four final state particles [two pions and two muons from the  $\Upsilon(nS) \rightarrow \mu^+\mu^-$ ] and initial state electron and positron.

The amplitude analysis of the  $e^+e^- \rightarrow \Upsilon(nS)\pi^+\pi^-$  transitions reported here is performed by means of an unbinned maximum likelihood fit. Before analyzing events in the signal region, one needs to determine the distribution of background events over the phase space. Samples of background events are selected in  $\Upsilon(nS)$  mass sidebands and then fit to the nominal mass of the corresponding  $\Upsilon(nS)$  state to match the phase space boundaries for the signal. Definitions of the mass sidebands and the event

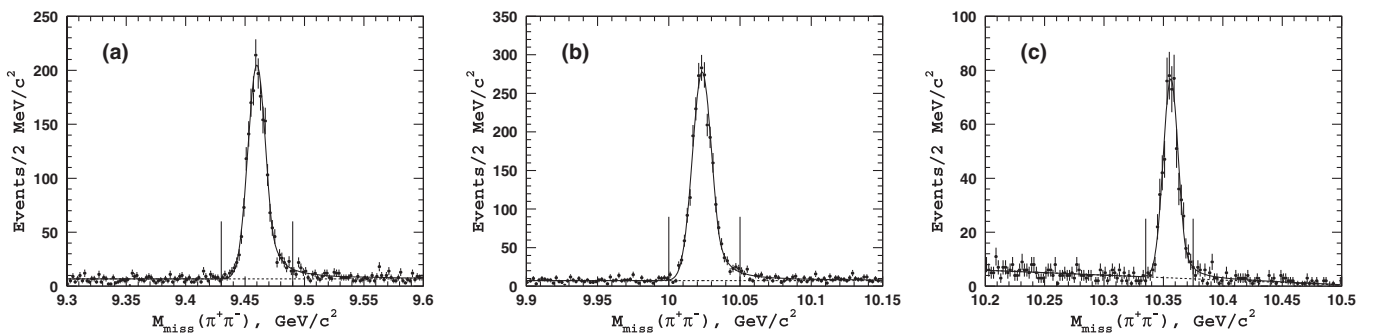


FIG. 2. Distribution of missing mass associated with the  $\pi^+\pi^-$  combination for  $e^+e^- \rightarrow \Upsilon(nS)\pi^+\pi^-$  candidate events in the (a)  $\Upsilon(1S)$ , (b)  $\Upsilon(2S)$ , (c)  $\Upsilon(3S)$  mass region. Points with error bars are the data, the solid line is the fit, and the dashed line shows the background component. Vertical lines define the corresponding signal region.

TABLE I. Summary of results from the analysis of the  $M_{\text{miss}}(\pi^+\pi^-)$  distribution. Quoted uncertainty is statistical only.

Final state	$\Upsilon(1S)\pi^+\pi^-$	$\Upsilon(2S)\pi^+\pi^-$	$\Upsilon(3S)\pi^+\pi^-$
$M(\pi^+\pi^-)$ Signal, $\text{GeV}/c^2$	$> 0.45$	$> 0.37$	$> 0.32$
$N_{\text{signal}}$	$2090 \pm 115$	$2476 \pm 97$	$628 \pm 41$
$\Upsilon$ Peak, $\text{MeV}/c^2$	$9459.9 \pm 0.8$	$10023.4 \pm 0.4$	$10356.2 \pm 0.7$
$\sigma$ , $\text{MeV}/c^2$	8.34	7.48	6.85
$M_{\text{miss}}(\pi^+\pi^-)$ Signal, $\text{GeV}/c^2$	(9.430, 9.490)	(10.000, 10.050)	(10.335, 10.375)
$N_{\text{events}}$	1905	2312	635
$f_{\text{sig}}$	$0.937 \pm 0.071$	$0.940 \pm 0.060$	$0.918 \pm 0.076$
$M_{\text{miss}}(\pi^+\pi^-)$ Sidebands, $\text{GeV}/c^2$	(9.38, 9.43) (9.49, 9.53)	(9.94, 9.99) (10.06, 10.11)	(10.30, 10.33) (10.38, 10.41)
$N_{\text{events}}$	272	291	91

yields are given in Table I. Dalitz plots for the sideband events are shown in Figs. 3(a), 3(b), and 3(c), where  $M(\Upsilon(nS)\pi)_{\text{max}}$  is the maximum invariant mass of the two  $\Upsilon(nS)\pi$  combinations; here the requirement on  $M(\pi^+\pi^-)$  is relaxed. For visualization purposes, we plot the Dalitz distributions in terms of  $M(\Upsilon(nS)\pi)_{\text{max}}$  in order to combine  $\Upsilon(nS)\pi^+$  and  $\Upsilon(nS)\pi^-$  events. As is apparent from these distributions, there is a strong enhancement in the

level of the background just above the  $\pi^+\pi^-$  invariant mass threshold. This enhancement is due to conversion of photons into an  $e^+e^-$  pair in the innermost parts of the Belle detector. Due to their low momenta, conversion electrons and positrons are poorly identified by the CDC and so pass the electron veto requirement. We exclude this high background region by applying a requirement on  $M(\pi^+\pi^-)$  as given in Table I. The distribution of

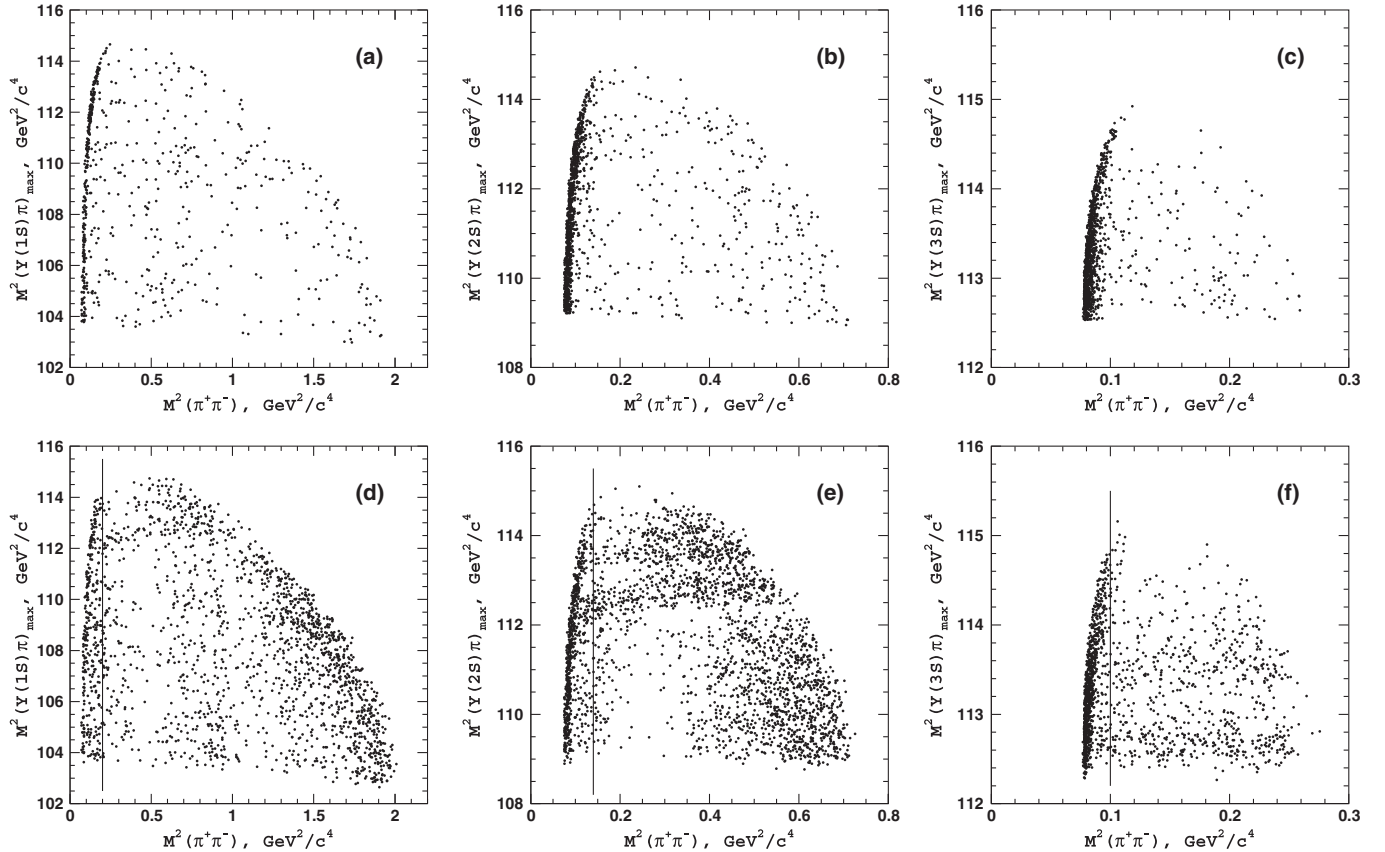


FIG. 3. Dalitz plots for  $\Upsilon(nS)\pi^+\pi^-$  events in sidebands of the (a)  $\Upsilon(1S)$ , (b)  $\Upsilon(2S)$ , and (c)  $\Upsilon(3S)$ . Dalitz plots for  $\Upsilon(nS)\pi^+\pi^-$  events in the signal region of the (d)  $\Upsilon(1S)$ , (e)  $\Upsilon(2S)$ , and (f)  $\Upsilon(3S)$ . Regions of the Dalitz plots to the left of the respective vertical line are excluded from the amplitude analyses.

background events in the remainder of the phase space is parametrized with the sum of a constant (that is uniform over phase space) and a term exponential in  $M^2(\pi^+\pi^-)$  to account for an excess of background events in the lower  $M^2(\pi^+\pi^-)$  region. In addition, in the  $\Upsilon(1S)\pi^+\pi^-$  sample, we include a contribution from  $\rho(770)^0 \rightarrow \pi^+\pi^-$  decays.

Figures 3(d), 3(e), and 3(f) show Dalitz plots for events in the signal regions for the three final states being considered here. In the fit to the  $e^+e^- \rightarrow \Upsilon(nS)\pi^+\pi^-$  data, we consider possible contributions from the following set of quasi-two-body modes:  $Z_b(10610)^\pm\pi^\mp$ ,  $Z_b(10650)^\pm\pi^\mp$ ,  $\Upsilon(nS)\sigma(500)$ ,  $\Upsilon(nS)f_0(980)$ ,  $\Upsilon(nS)f_2(1270)$ , and a nonresonant component. The transition amplitude  $\mathcal{M}_{\Upsilon\pi\pi}$  is written as a coherent sum of these components,

$$\mathcal{M}_{\Upsilon\pi\pi} = \mathcal{A}_{Z_1\pi} + \mathcal{A}_{Z_2\pi} + \mathcal{A}_{\Upsilon\sigma} + \mathcal{A}_{\Upsilon f_0} + \mathcal{A}_{\Upsilon f_2} + \mathcal{A}_{\text{NR}}. \quad (2)$$

Including  $\sigma(500)$  in the amplitude improves the description of  $\Upsilon(1S)\pi^+\pi^-$  data in the low  $\pi^+\pi^-$  mass region as compared to our previous analysis [3]. Mass and width of  $\sigma(500)$  are poorly defined from the data and are fixed at 600 MeV/ $c^2$  and 400 MeV, respectively. The effect of this limitation on the fit results is included in systematic studies. Mass and coupling constants of the  $f_0(980)$  state are fixed at values defined from the analysis of  $B^+ \rightarrow K^+\pi^+\pi^-$ :  $M(f_0(980)) = 950$  MeV/ $c^2$ ,  $g_{\pi\pi} = 0.23$ ,  $g_{KK} = 0.73$  [12]. The mass and width are fixed at world average values [13]. Parameters of  $Z_b$  states are determined from the fit to data. A detailed description of the amplitude is given in the Appendix.

For modes with higher  $\Upsilon(nS)$  states, the available phase space is very limited, making it impossible to distinguish unambiguously between multiple scalar components in the amplitude. In these cases we fit the data with an amplitude given by Eq. (A4); components with statistical significance below  $3\sigma$  are then fixed at zero and the fit is repeated. As a result, in the nominal model used to fit the  $e^+e^- \rightarrow \Upsilon(2S)\pi^+\pi^-$  data, we exclude the  $f_0(980)$  amplitude. In addition, in the nominal model used to fit the  $e^+e^- \rightarrow \Upsilon(3S)\pi^+\pi^-$  data, we also exclude the  $\sigma(500)$  and  $f_2(1270)$  components. Possible contributions from higher mass scalar states are effectively accommodated by a constant term of the nonresonant amplitude. The total numbers of fit parameters are 16, 14, and 10 for the final states with  $\Upsilon(1S)$ ,  $\Upsilon(2S)$ , and  $\Upsilon(3S)$ , respectively. The effect of this reduction of the amplitude is considered in the evaluation of the systematic uncertainties.

In the fit to the data, we test the following assumptions on the spin and parity of the observed  $Z_b$  states:  $J^P = 1^+$ ,  $1^-$ ,  $2^+$  and  $2^-$ . Note that  $J^P = 0^+$  and  $0^-$  combinations are forbidden because of the observed  $Z_b \rightarrow \Upsilon(nS)\pi$  and  $Z_b \rightarrow h_b(mP)\pi$  decay modes, respectively. [Since the masses and the widths of two resonances measured in

the  $h_b(mP)\pi$  and in the  $\Upsilon(nS)\pi$  [3] systems are consistent, we assume the same pair of  $Z_b$  states is observed in these decay modes.] The simplified angular analysis reported in Ref. [5] favors the  $J^P = 1^+$  hypothesis; thus, our nominal model here adopts  $J^P = 1^+$ .

The logarithmic likelihood function  $\mathcal{L}$  is an incoherent sum of a signal  $S$  and background  $B$  terms,

$$\mathcal{L} = -2 \sum_{\text{events}} \ln(f_{\text{sig}}S + (1 - f_{\text{sig}})B), \quad (3)$$

where the summation is performed over all selected candidate events and  $f_{\text{sig}}$  is the fraction of signal events in the data sample (see Table I). The  $S$  term in Eq. (3) is formed from  $|\mathcal{M}_{\Upsilon\pi\pi}|^2$  [see Eq. (A4) of the Appendix] convolved with the detector resolution, and the background density function  $B$  is determined from the fit to the sideband events. Both  $S$  and  $B$  are normalized to unity.

For normalization, we use a large sample of signal  $e^+e^- \rightarrow \Upsilon(nS)\pi^+\pi^- \rightarrow \mu^+\mu^-\pi^+\pi^-$  MC events generated with a uniform distribution over the phase space and processed through the full detector simulation. The simulation also accounts for the beam energy spread of  $\sigma = 5.3$  MeV and c.m. energy variations throughout the data taking period. The use of the full MC events for the normalization allows us to account for variations of the reconstruction efficiency over the phase space. More details can be found in Ref. [14]. Results of fits to  $\Upsilon(nS)\pi^+\pi^-$  events in the signal regions with the nominal model are shown in Fig. 4, where one-dimensional projections of the data and fits are presented. In order to combine  $Z_b^+$  and  $Z_b^-$  signals, we plot the  $M(\Upsilon(nS)\pi)_{\text{max}}$  distribution rather than individual  $M(\Upsilon(nS)\pi^+)$  and  $M(\Upsilon(nS)\pi^-)$  spectra.

A more detailed comparison of the fit results and the data is shown in Figs. 5–7, where mass projections for various regions of the Dalitz plots are presented. In addition, comparison of the angular distributions for the  $\Upsilon(1S)\pi^+\pi^-$  final state in the  $Z_b$  signal region [ $M(\Upsilon(nS)\pi)_{\text{max}} > 10590$  MeV/ $c^2$ ] and the nonresonant region [ $M(\Upsilon(nS)\pi)_{\text{max}} < 10550$  MeV/ $c^2$ ] are shown in Fig. 8. For  $\Upsilon(2S)\pi^+\pi^-$  and  $\Upsilon(3S)\pi^+\pi^-$  final states, we define the  $Z_b(10610)$  region [ $10605$  MeV/ $c^2 < M(\Upsilon(nS)\pi)_{\text{max}} < 10635$  MeV/ $c^2$ ], the  $Z_b(10650)$  region [ $10645$  MeV/ $c^2 < M(\Upsilon(nS)\pi)_{\text{max}} < 10675$  MeV/ $c^2$ ], and the nonresonant region [ $M(\Upsilon(nS)\pi)_{\text{max}} < 10570$  MeV/ $c^2$ ]. Corresponding angular distributions are presented in Figs. 9 and 10.

To quantify the goodness of fits, we utilize various approaches. We use a mixed sample technique described in detail in Ref. [15]. The two samples being combined are the experimental data and MC samples generated with the nominal model including background. The statistics in each MC sample is 10 times that of the experiment. This technique allows us to test if two data samples share the same parent distribution. Its power is equivalent to that of

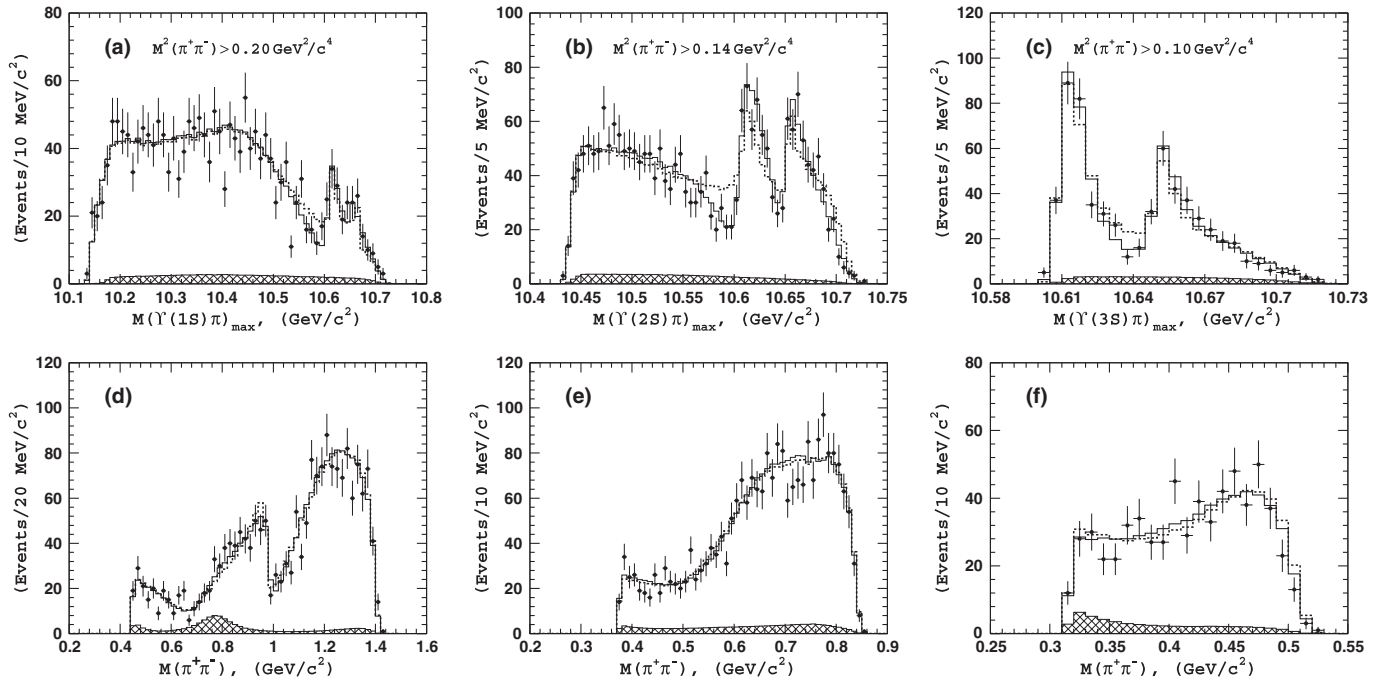


FIG. 4. Comparison of fit results with the nominal model with  $J^P = 1^+$  assigned to both  $Z_b$  states (solid open histogram) and the data (points with error bars) for events in the (a),(d)  $\Upsilon(1S)\pi^+\pi^-$ , (b),(e)  $\Upsilon(2S)\pi^+\pi^-$ , and (c),(f)  $\Upsilon(3S)\pi^+\pi^-$  signal region. The dashed histogram shows results of the fit with a  $J^P = 2^+$  assignment for the  $Z_b$  states. Hatched histograms show the estimated background components.

the  $\chi^2$  test for data with enough statistics and is applicable for multidimensional fits with a small data sample. From this analysis, we find that the nominal model and the data are consistent at 27%, 61%, and 34% confidence levels for

the  $\Upsilon(1S)\pi^+\pi^-$ ,  $\Upsilon(2S)\pi^+\pi^-$ , and  $\Upsilon(3S)\pi^+\pi^-$  final states, respectively.

As an alternative approach, we calculate  $\chi^2$  values for one-dimensional projections shown in Fig. 4, combining

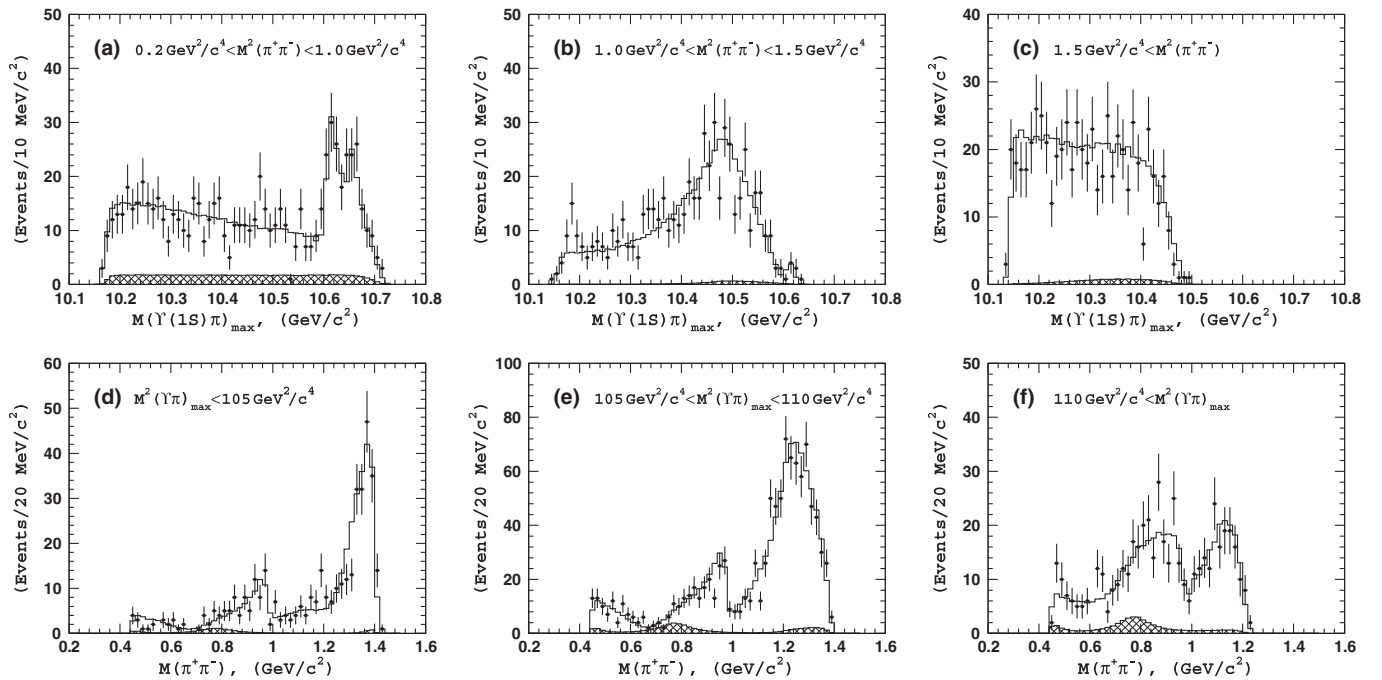


FIG. 5. A detailed comparison of fit results with the nominal model (open histogram) with the data (points with error bars) for events in the  $\Upsilon(1S)\pi^+\pi^-$  signal region. Hatched histograms show the estimated background components. Panels (a)–(c) show  $M(\Upsilon(1S)\pi)_{\max}$  projections in different  $M^2(\pi^+\pi^-)$  regions. Panels (d)–(f) show  $M(\pi^+\pi^-)$  projections in different  $M^2(\Upsilon(1S)\pi)_{\max}$  regions.



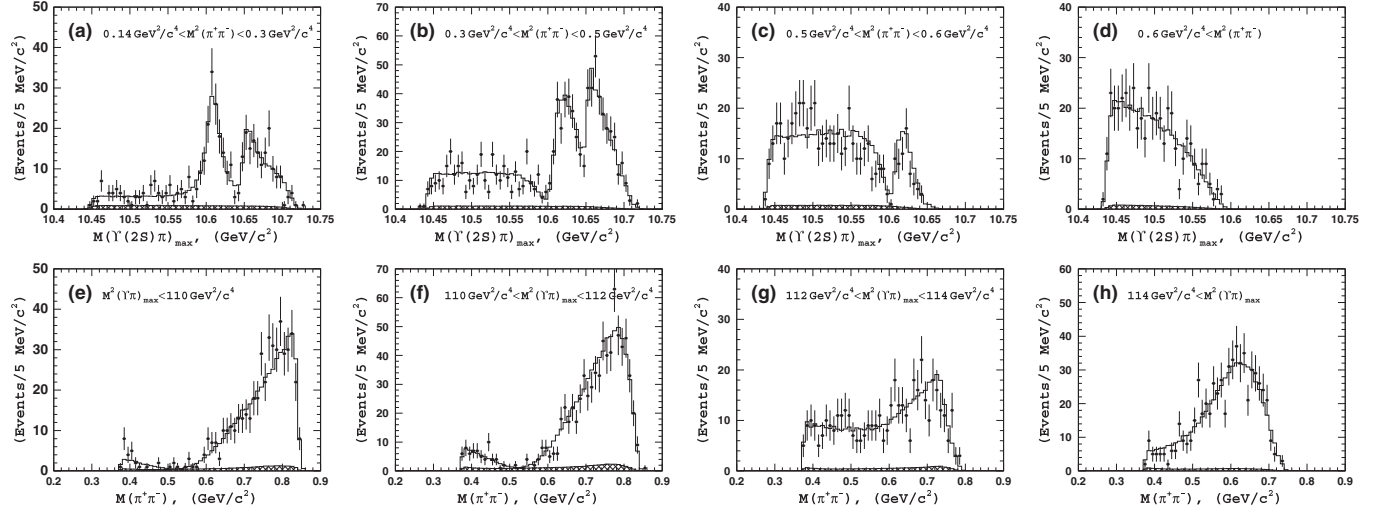


FIG. 6. A detailed comparison of fit results with the nominal model (open histogram) with the data (points with error bars) for events in the  $\Upsilon(2S)\pi^+\pi^-$  signal region. Hatched histograms show the estimated background components. Panels (a)–(d) show  $M(\Upsilon(2S)\pi)_{\max}$  projections in different  $M^2(\pi^+\pi^-)$  regions. Panels (e)–(h) show  $M(\pi^+\pi^-)$  projections in different  $M^2(\Upsilon(2S)\pi)_{\max}$  regions.

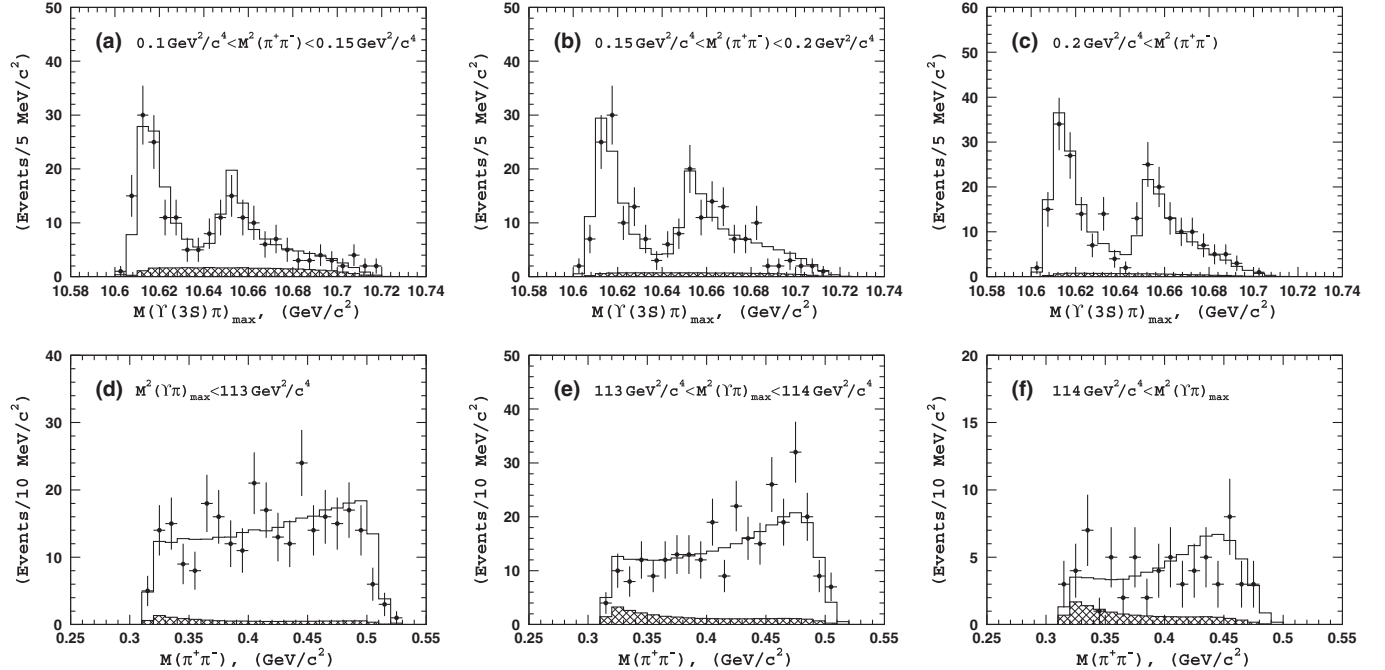


FIG. 7. A detailed comparison of fit results with the nominal model (open histogram) with the data (points with error bars) for events in the  $\Upsilon(3S)\pi^+\pi^-$  signal region. Hatched histograms show the estimated background components. Panels (a)–(c) show  $M(\Upsilon(3S)\pi)_{\max}$  projections in different  $M^2(\pi^+\pi^-)$  regions. Panels (d)–(f) show  $M(\pi^+\pi^-)$  projections in different  $M^2(\Upsilon(3S)\pi)_{\max}$  regions.

any bin with fewer than nine events with its neighbor. A  $\chi^2$  variable for the multinomial distribution is then calculated as

$$\chi^2 = -2 \sum_{i=1}^{N_{\text{bins}}} n_i \ln \left( \frac{p_i}{n_i} \right), \quad (4)$$

where  $n_i$  is the number of events observed in the  $i$ th bin and  $p_i$  is the number of events expected from the model. For a large number of events, this formulation becomes equivalent to the standard  $\chi^2$  definition. Since we are minimizing the unbinned likelihood function, such a constructed  $\chi^2$  variable does not asymptotically follow a typical  $\chi^2$  distribution but is rather bounded by two  $\chi^2$  distributions

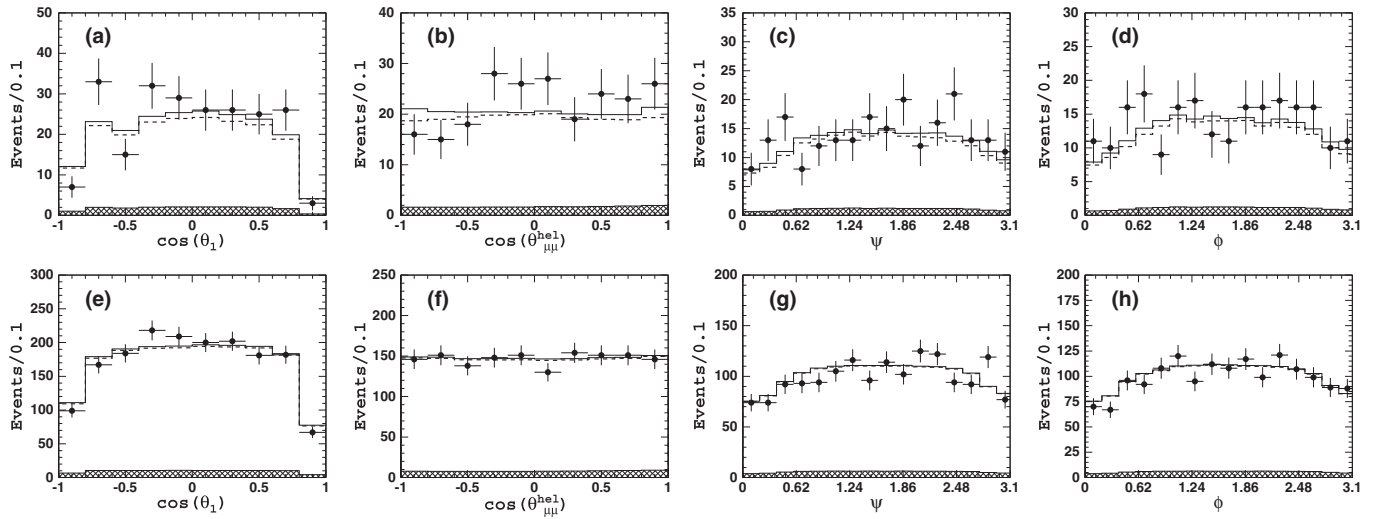


FIG. 8. Comparison of angular distributions for signal  $\Upsilon(1S)\pi^+\pi^-$  events in data (points with error bars), fit with the nominal model with  $J^P = 1^+$  (open histogram), and fit with the  $J^P = 2^+$  model (dashed histogram). Hatched histograms show the estimated background components. The top row is for the combined  $Z_b(10610)$  and  $Z_b(10650)$  region and the bottom row is for the non-resonant region. See text for details.

with  $(N_{\text{bins}} - 1)$  and  $(N_{\text{bins}} - k - 1)$  degrees of freedom [16], where  $k$  is the number of fit parameters. Because it is bounded by two  $\chi^2$  distributions, it remains a useful statistic to estimate the goodness of the fits. Results are presented in

Table II. For all final states, the nominal model provides a good description of the data.

We find that the model with  $J^P = 1^+$  assigned to both  $Z_b$  states provides the best description of the data for all

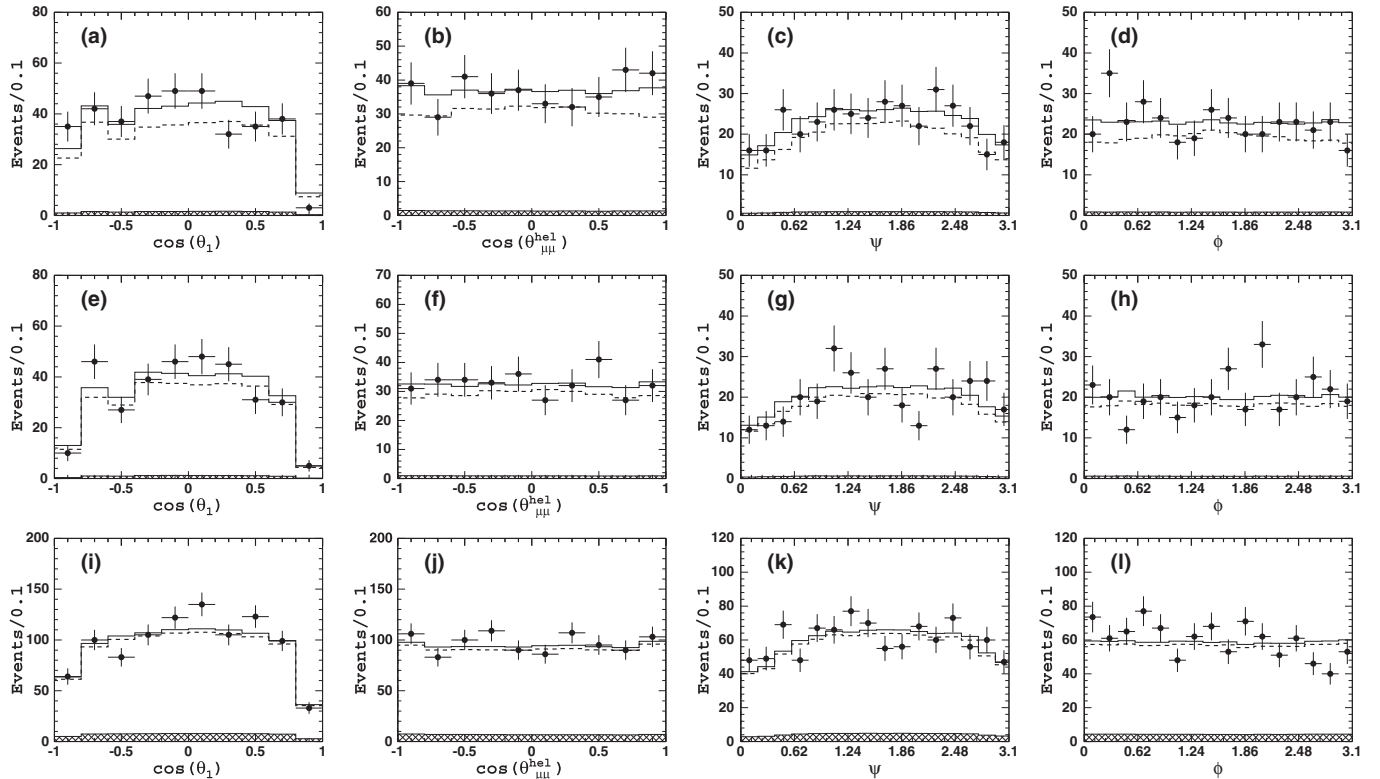


FIG. 9. Comparison of angular distributions for signal  $\Upsilon(2S)\pi^+\pi^-$  events in data (points with error bars), fit with the nominal model with  $J^P = 1^+$  (open histogram), and fit with the  $J^P = 2^+$  model (dashed histogram). Hatched histograms show the estimated background components. The top row is for the  $Z_b(10610)$  region, the middle row is for the  $Z_b(10650)$  region and the bottom row is for the non-resonant region. See text for details.

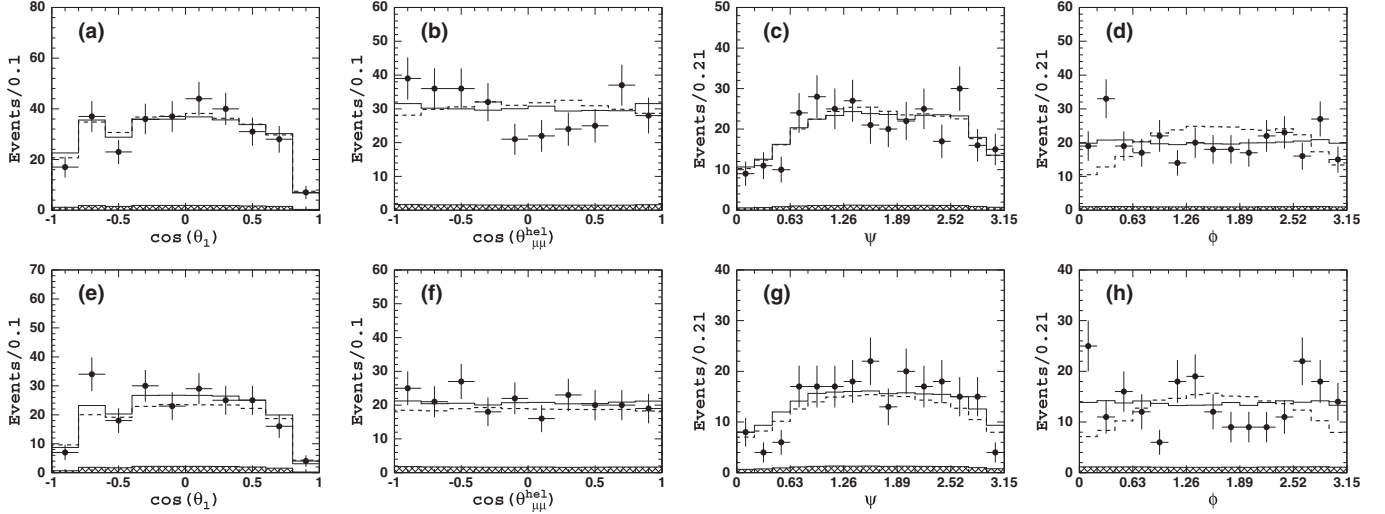


FIG. 10. Comparison of angular distributions for signal  $\Upsilon(3S)\pi^+\pi^-$  events in data (points with error bars), fit with the nominal model with  $J^P = 1^+$  (open histogram), and fit with the  $J^P = 2^+$  model (dashed histogram). Hatched histograms show the estimated background components. The top row is for the  $Z_b(10610)$  region and the bottom row is for the  $Z_b(10650)$  region. See text for details.

final states. Fits to the data with alternative  $J^P$  values assigned to the two  $Z_b$  states are compared with the nominal one in terms of the likelihood values returned by the fits. For each model, we calculate  $\Delta\mathcal{L} = \mathcal{L}(J^P) - \mathcal{L}_0$  which is the difference in the likelihood values returned by the fit to a model with an alternative  $J^P$  assignment and the nominal one. Results of this study for the  $\Upsilon(2S)\pi^+\pi^-$  and  $\Upsilon(3S)\pi^+\pi^-$  modes (where the  $Z_b\pi$  signal comprises a significant fraction of the three-body signal) are summarized in Table III. For the  $\Upsilon(1S)\pi^+\pi^-$  mode, we fit the data only to models with the same  $J^P$  assigned to both  $Z_b$  states. The obtained  $\Delta\mathcal{L}$  values are 64, 41, and 59 for the  $J^P = 1^-$ ,  $2^+$ , and  $2^-$  models, respectively.

The discrimination power is found to be mainly due to an interference term between the  $Z_b$  and the underlying non- $Z_b$  amplitudes. The best discrimination is provided by the  $e^+e^- \rightarrow \Upsilon(2S)\pi^+\pi^-$  channel, where the two components are comparable in size, thus maximizing the relative size of the interference term. To cross-check the separation power, we perform a MC study in which we generate a large number of  $\Upsilon(nS)\pi^+\pi^-$  samples, each with statistics equivalent to the data, and perform fits of each pseudo-experiment with different  $J^P$  models. The obtained  $\Delta\mathcal{L}$  distributions are fit to a Gaussian function

(a bifurcated Gaussian function for asymmetric distributions) to estimate the probability to find  $\Delta\mathcal{L}$  larger than the value in data. We find that alternative models with the same  $J^P$  assigned to both  $Z_b$  states are rejected at a level exceeding 8 standard deviations using the  $Ud\pi^+\pi^-$  channel only. The comparisons of the fit result where both  $Z_b$  are assumed to be  $J^P = 2^+$  states (the next best hypothesis) and the data are shown in Figs. 4 and 8–10.

In fits with different  $J^P$  values assigned to the  $Z_b(10610)$  and  $Z_b(10650)$  states, the smallest  $\Delta\mathcal{L}$  value is provided by the model with  $Z_b(10610)$  assumed to be a  $1^+$  state and  $Z_b(10650)$  a  $2^+$  state, as shown in Table III. A similar study with MC pseudo-experiments shows that this alternative hypothesis is rejected at a level exceeding 6 standard deviations.

Finally, we note that multiple solutions are found in the fit to the  $\Upsilon(1S)\pi^+\pi^-$  and  $\Upsilon(2S)\pi^+\pi^-$  final states. This is due to the presence of several  $S$ -wave components in the three-body amplitudes for these modes. While the overall fraction of the  $S$ -wave contribution is a well-defined

TABLE II. Results of the  $\chi^2/n_{\text{bins}}$  calculations for one-dimensional projections shown in Fig. 4.

	$\Upsilon(1S)\pi^+\pi^-$	$\Upsilon(2S)\pi^+\pi^-$	$\Upsilon(3S)\pi^+\pi^-$
$M(\Upsilon\pi)_{\text{max}}$	61.5/53	46.6/54	12.0/20
$M(\pi^+\pi^-)$	68.3/49	45.1/48	18.6/20

TABLE III. Results of the fit to  $\Upsilon(2S)\pi^+\pi^-$  [ $\Upsilon(3S)\pi^+\pi^-$ ] events with different  $J^P$  values assigned to the  $Z_b(10610)$  and  $Z_b(10650)$  states. Shown in the table is the difference in  $\mathcal{L}$  values for fits to an alternative model and the nominal one.

$Z_b(10610)$	$Z_b(10650)$			
	$1^+$	$1^-$	$2^+$	$2^-$
$1^+$	0(0)	60(33)	42(33)	77(63)
$1^-$	226(47)	264(73)	224(68)	277(106)
$2^+$	205(33)	235(104)	207(87)	223(128)
$2^-$	289(99)	319(111)	321(110)	304(125)

TABLE IV. Results on cross sections for three-body  $e^+e^- \rightarrow \Upsilon(nS)\pi^+\pi^-$  transitions. The first quoted error is statistical and the second is systematic. The last line quotes results from our previous publication for comparison.

Final state	$\Upsilon(1S)\pi^+\pi^-$	$\Upsilon(2S)\pi^+\pi^-$	$\Upsilon(3S)\pi^+\pi^-$
Signal yield	$2090 \pm 115$	$2476 \pm 97$	$628 \pm 41$
Efficiency, %	45.9	39.0	24.4
$\mathcal{B}_{\Upsilon(nS) \rightarrow \mu^+\mu^-}$ , % [13]	$2.48 \pm 0.05$	$1.93 \pm 0.17$	$2.18 \pm 0.21$
$\sigma_{e^+e^- \rightarrow \Upsilon(nS)\pi^+\pi^-}^{\text{vis}}$ , pb	$1.51 \pm 0.08 \pm 0.09$	$2.71 \pm 0.11 \pm 0.30$	$0.97 \pm 0.06 \pm 0.11$
$\sigma_{e^+e^- \rightarrow \Upsilon(nS)\pi^+\pi^-}$ , pb	$2.29 \pm 0.12 \pm 0.14$	$4.11 \pm 0.16 \pm 0.45$	$1.47 \pm 0.09 \pm 0.16$
$\sigma_{e^+e^- \rightarrow \Upsilon(nS)\pi^+\pi^-}^{\text{vis}}$ , pb [1]	$1.61 \pm 0.10 \pm 0.12$	$2.35 \pm 0.19 \pm 0.32$	$1.44_{-0.45}^{+0.55} \pm 0.19$

quantity, the individual components are strongly correlated and thus poorly separated by the fit. Because of this effect, we do not present relative phases and fractions of individual  $S$ -wave contributions except for the  $\Upsilon(1S)f_0(980)$  mode, whose parameters are well defined due to a prominent interference pattern. The effect of multiple solutions on other fit parameters is included as a systematic uncertainty.

## V. RESULTS

The cross sections of the three-body  $e^+e^- \rightarrow \Upsilon(nS)\pi^+\pi^-$  processes are calculated using the following formula:

$$\begin{aligned} \sigma_{e^+e^- \rightarrow \Upsilon(nS)\pi^+\pi^-} &= \frac{\sigma_{e^+e^- \rightarrow \Upsilon(nS)\pi^+\pi^-}^{\text{vis}}}{1 + \delta_{\text{ISR}}} \\ &= \frac{N_{\Upsilon(nS)\pi^+\pi^-}}{L \cdot \mathcal{B}_{\Upsilon(nS) \rightarrow \mu^+\mu^-} \cdot \varepsilon_{\Upsilon(nS)\pi^+\pi^-} (1 + \delta_{\text{ISR}})}, \end{aligned} \quad (5)$$

where  $\sigma_{\text{vis}}$  is the visible cross section. The ISR correction factor  $(1 + \delta_{\text{ISR}}) = 0.659 \pm 0.015$  is determined using formulas given in Ref. [17], where we use the  $e^+e^- \rightarrow \Upsilon(2S)\pi^+\pi^-$  cross section measured in Ref. [18]. The quoted uncertainty in the ISR correction factor is due to uncertainty in the  $\Upsilon(10860)$  parameters, assumption on the nonresonance component and selection criteria. The integrated luminosity is measured to be  $L = 121.4 \text{ fb}^{-1}$ , and the reconstruction efficiency  $\varepsilon_{\Upsilon(nS)\pi^+\pi^-}$  (including trigger efficiency and final state radiation) is determined from the signal MC events generated according to the nominal model from the amplitude analysis. For the branching fractions of the  $\Upsilon(nS) \rightarrow \mu^+\mu^-$  decays, the world average values are used [13]. Results of the calculations are summarized in Table IV. The Born cross section can be obtained by multiplying Eq. (5) by the vacuum polarization correction factor,  $|1 - \Pi|^2 = 0.9286$  [19]. The  $\Upsilon(10860) \rightarrow \Upsilon(nS)\pi^+\pi^-$  branching fractions listed in Ref. [13] can be obtained by dividing our results for  $\sigma^{\text{vis}}$  in Table IV by the  $e^+e^- \rightarrow b\bar{b}$  cross section measured at the  $\Upsilon(10860)$  peak,  $\sigma_{e^+e^- \rightarrow b\bar{b}}(\sqrt{s} = 10866) = 0.340 \pm 0.016 \text{ nb}$  [20].

The dominant sources of systematic uncertainties contributing to the measurements of cross sections for the three-body  $e^+e^- \rightarrow \Upsilon(nS)\pi^+\pi^-$  transitions are given in Table V. The uncertainty in the signal yield is estimated by varying fit parameters within 1 standard deviation one by one and repeating the fit to the corresponding  $M_{\text{miss}}(\pi^+\pi^-)$  distribution. The uncertainty in the muon identification is determined using a large sample of  $J/\psi \rightarrow \mu^+\mu^-$  events in data and MC and is found to be 1% per muon. The uncertainty in tracking efficiency is estimated using partially reconstructed  $D^{*-} \rightarrow \pi^- D^0 [K_S^0 \pi^+ \pi^-]$  events and it is found to be 0.35% per a high momentum track (muons from  $\Upsilon(nS) \rightarrow \mu^+\mu^-$  decays) and 1% per a lower momentum track (pions). The uncertainty in the radiative correction factor is determined from a dedicated study. It is found to be due mainly to the uncertainty in the parametrization of the energy dependence of the  $e^+e^- \rightarrow \Upsilon(nS)\pi^+\pi^-$  cross section, the uncertainty in the c.m. energy and the selection criteria. All contributions are added in quadrature to obtain the overall systematic uncertainty of 6.2%, 10.9%, and 11.4% for  $n = 1, 2$ , and 3, respectively. Our results for  $\sigma_{\text{vis}}(e^+e^- \rightarrow \Upsilon(nS)\pi^+\pi^-)$  may be compared with the previous measurements by Belle performed with a data sample of  $21 \text{ fb}^{-1}$  [1] (see last line in Table IV). We find that the two sets of measurements are consistent within uncertainties.

Results of the amplitude analysis are summarized in Table VI, where fractions of individual quasi-two-body

 TABLE V. List of dominant sources of systematic uncertainties (in percent) contributing to the measurement of three-body  $e^+e^- \rightarrow \Upsilon(nS)\pi^+\pi^-$  cross sections.

Final state	$\Upsilon(1S)\pi^+\pi^-$	$\Upsilon(2S)\pi^+\pi^-$	$\Upsilon(3S)\pi^+\pi^-$
$\mathcal{B}_{\Upsilon(nS) \rightarrow \mu^+\mu^-}$ , [13]	2.0	8.8	9.6
Signal yield	4.5	5.3	4.9
Muon ID	2.0	2.0	2.0
Tracking	2.7	2.7	2.7
ISR correction	2.0	2.0	2.0
Luminosity	1.4	1.4	1.4
Total	6.2	10.9	11.4

TABLE VI. Summary of results of fits to  $\Upsilon(nS)\pi^+\pi^-$  events in the signal regions.

Parameter	$\Upsilon(1S)\pi^+\pi^-$	$\Upsilon(2S)\pi^+\pi^-$	$\Upsilon(3S)\pi^+\pi^-$
$f_{Z_b^\mp(10610)\pi^\pm}$ , %	$4.8 \pm 1.2^{+1.5}_{-0.3}$	$18.1 \pm 3.1^{+4.2}_{-0.3}$	$30.0 \pm 6.3^{+5.4}_{-7.1}$
$Z_b(10610)$ mass, MeV/ $c^2$	$10608.5 \pm 3.4^{+3.7}_{-1.4}$	$10608.1 \pm 1.2^{+1.5}_{-0.2}$	$10607.4 \pm 1.5^{+0.8}_{-0.2}$
$Z_b(10610)$ width, MeV	$18.5 \pm 5.3^{+6.1}_{-2.3}$	$20.8 \pm 2.5^{+0.3}_{-2.1}$	$18.7 \pm 3.4^{+2.5}_{-1.3}$
$f_{Z_b^\mp(10650)\pi^\pm}$ , %	$0.87 \pm 0.32^{+0.16}_{-0.12}$	$4.05 \pm 1.2^{+0.95}_{-0.15}$	$13.3 \pm 3.6^{+2.6}_{-1.4}$
$Z_b(10650)$ mass, MeV/ $c^2$	$10656.7 \pm 5.0^{+1.1}_{-3.1}$	$10650.7 \pm 1.5^{+0.5}_{-0.2}$	$10651.2 \pm 1.0^{+0.4}_{-0.3}$
$Z_b(10650)$ width, MeV	$12.1^{+11.3+2.7}_{-4.8-0.6}$	$14.2 \pm 3.7^{+0.9}_{-0.4}$	$9.3 \pm 2.2^{+0.3}_{-0.5}$
$\phi_Z$ , degrees	$67 \pm 36^{+24}_{-52}$	$-10 \pm 13^{+34}_{-12}$	$-5 \pm 22^{+15}_{-33}$
$c_{Z_b(10650)}/c_{Z_b(10610)}$	$0.40 \pm 0.12^{+0.05}_{-0.11}$	$0.53 \pm 0.07^{+0.32}_{-0.11}$	$0.69 \pm 0.09^{+0.18}_{-0.07}$
$f_{\Upsilon(nS)f_2(1270)}$ , %	$14.6 \pm 1.5^{+6.3}_{-0.7}$	$4.09 \pm 1.0^{+0.33}_{-1.0}$	—
$f_{\Upsilon(nS)(\pi^+\pi^-)_S}$ , %	$86.5 \pm 3.2^{+3.3}_{-4.9}$	$101.0 \pm 4.2^{+6.5}_{-3.5}$	$44.0 \pm 6.2^{+1.8}_{-4.3}$
$f_{\Upsilon(nS)f_0(980)}$ , %	$6.9 \pm 1.6^{+0.8}_{-2.8}$	—	—

modes, masses and widths of the two  $Z_b$  states, the relative phase  $\phi_Z$  between the two  $Z_b$  amplitudes and fraction  $c_{Z_{10610}}/c_{Z_{10650}}$  of their amplitudes are given. The fraction  $f_X$  of the total three-body signal attributed to a particular quasi-two-body intermediate state is calculated as

$$f_X = \frac{\int |\mathcal{A}_X|^2 d\Omega}{\int |\mathcal{M}_{\Upsilon(nS)\pi\pi}|^2 d\Omega}, \quad (6)$$

where  $\mathcal{A}_X$  is the amplitude for a particular component  $X$  of the three-body amplitude  $\mathcal{M}_{\Upsilon(nS)\pi\pi}$ , defined in the Appendix. For amplitudes where the  $\pi^+\pi^-$  system is in an  $S$ -wave, we do not calculate individual fractions for every component but present the result only for the combination  $\Upsilon(nS)(\pi^+\pi^-)_S$  of all such components. The only exception is made for the  $\Upsilon(1S)f_0(980)$  component. The statistical significance of this signal, determined as  $\sqrt{\mathcal{L}_{f_0} - \mathcal{L}_0}$ , where  $\mathcal{L}_{f_0}$  is the likelihood value with the  $f_0(980)$  amplitude fixed at zero, exceeds 8 standard deviations. Note that the sum of the fit fractions for all components is not necessarily unity because of the interference. Statistical uncertainties for relative fractions of intermediate channels quoted in Table VI are determined utilizing a MC pseudo-experiment technique. For each three-body final state, we generate a large number of MC samples, each with statistics equivalent to the experimental data (including background) and with a phase space distribution according to the nominal model. Each MC sample is then fit to the nominal model, and fractions  $f_i$  of contributing submodes are determined. The standard deviation of the  $f_i$  distribution is then taken as the statistical uncertainty for the fraction of the corresponding submode; see Table VI.

Combining results for the three-body cross sections from Table IV with the results of the amplitude analysis from

Table VI, we calculate the product  $\sigma_{Z_b^\pm\pi^\mp} \times \mathcal{B}_{\Upsilon(nS)\pi^\mp}$ , where  $\sigma_{Z_b^\pm\pi^\mp}$  is the cross section of the  $e^+e^-$  annihilation to  $Z_b^\pm\pi^\mp$  and  $\mathcal{B}_{\Upsilon(nS)\pi^\mp}$  is the branching fraction of  $Z_b^\pm$  decay to  $\Upsilon(nS)\pi^\pm$ :

$$\begin{aligned} \sigma_{Z_b^\pm(10610)\pi^\mp} \times \mathcal{B}_{\Upsilon(1S)\pi^\mp} &= 110 \pm 27^{+36}_{-10} \text{ fb} \\ \sigma_{Z_b^\pm(10610)\pi^\mp} \times \mathcal{B}_{\Upsilon(2S)\pi^\mp} &= 744 \pm 127^{+190}_{-86} \text{ fb} \\ \sigma_{Z_b^\pm(10610)\pi^\mp} \times \mathcal{B}_{\Upsilon(3S)\pi^\mp} &= 442 \pm 93^{+93}_{-115} \text{ fb} \\ \sigma_{Z_b^\pm(10650)\pi^\mp} \times \mathcal{B}_{\Upsilon(1S)\pi^\mp} &= 20 \pm 7^{+4}_{-3} \text{ fb} \\ \sigma_{Z_b^\pm(10650)\pi^\mp} \times \mathcal{B}_{\Upsilon(2S)\pi^\mp} &= 167 \pm 49^{+43}_{-21} \text{ fb} \\ \sigma_{Z_b^\pm(10650)\pi^\mp} \times \mathcal{B}_{\Upsilon(3S)\pi^\mp} &= 196 \pm 54^{+43}_{-25} \text{ fb}. \end{aligned} \quad (7)$$

The main sources of systematic uncertainties in the amplitude analysis are as follows.

- (i) The uncertainty in parametrization of the transition amplitude. To estimate this uncertainty, we use various modifications of the nominal model and repeat the fit to the data. In particular, for the  $\Upsilon(1S)\pi^+\pi^-$  and  $\Upsilon(2S)\pi^+\pi^-$  channels, we modify the parametrization of the nonresonant amplitude, replacing the  $s_{23}$  dependence from linear to a  $\sqrt{s_{23}}$  form and replacing the  $\Upsilon(nS)f_2(1270)$  amplitude with a  $D$ -wave component in the nonresonant amplitude. For the  $\Upsilon(3S)\pi^+\pi^-$  channel, we modify the nominal model by adding various components of the amplitude initially fixed at zero: a  $\Upsilon(3S)f_2(1270)$  component with an amplitude and phase fixed from the fit to the  $\Upsilon(1S)\pi^+\pi^-$  channel. We also fit the  $\Upsilon(3S)\pi^+\pi^-$  data with the nonresonant amplitude set to be uniform. To estimate dependence on parametrization of the  $Z_b\pi$  amplitudes, we repeat the fit to the data with a  $Z_b$  line

shape parametrized by a Flatté function with a coupled channel being  $B\bar{B}^* + \text{c.c.}$  and  $B^*\bar{B}$  for the  $Z_b(10610)$  and  $Z_b(10650)$ , respectively. Finally, we fit the data with the mass and width of  $\sigma(500)$  state floating. In this case the fit to the  $\Upsilon(1S)\pi^+\pi^-$  data returns the value of  $630 \pm 420 \text{ MeV}/c^2$  for the mass and  $730 \pm 560 \text{ MeV}$  for the width. Variations in fit parameters and fractions of contributing channels determined from fits with these models are taken as an estimation of the model-related uncertainty [below 12% for  $\Upsilon(2S)\pi^+\pi^-$  and  $\Upsilon(3S)\pi^+\pi^-$ , up to 30% for  $\Upsilon(1S)\pi^+\pi^-$ ].

- (ii) Multiple solutions found for the  $\Upsilon(1S)\pi^+\pi^-$  and  $\Upsilon(2S)\pi^+\pi^-$  modes are treated as a model-related uncertainty, with variations in fit parameters included in the systematic uncertainty (up to 9%).
- (iii) Uncertainty in the c.m. energy leads to uncertainty in the phase space boundaries. To estimate the associated effect on fit parameters, we generate a normalization phase space MC sample that corresponds to  $E_{\text{cm}} \pm 3 \text{ MeV}$ , where  $E_{\text{cm}}$  is the nominal c.m. energy, and we refit [below 3% for  $\Upsilon(1S)\pi^+\pi^-$  and  $\Upsilon(2S)\pi^+\pi^-$  and up to 8% for  $\Upsilon(3S)\pi^+\pi^-$ ].
- (iv) Uncertainty in the fraction of signal events  $f_{\text{sig}}$  in the sample. To determine the associated uncertainties in fit parameters we vary  $f_{\text{sig}}$  within its error and repeat the fit to the data. We also fit the data with  $f_{\text{sig}}$  relaxed (from 4% to 7%).
- (v) Uncertainty in the parametrization of the distribution of background events. We repeat the fit to the data with a background density set to be uniform over the phase space (from 3% to 5%).
- (vi) Uncertainty associated with a requirement on  $M(\pi^+\pi^-)$ . To estimate the effect, we remove this requirement and repeat the analysis (below 6%).
- (vii) Uncertainty associated with the fitting procedure. This is estimated from MC studies (below 4%).

The relative contribution of each particular source of the systematic uncertainty to the overall value depends on the three-body  $\Upsilon(nS)\pi^+\pi^-$  channel and on the particular mode. Systematic uncertainties in all parameters determined from the fit to the  $\Upsilon(1S)\pi^+\pi^-$  data are dominated by model-related uncertainties. Contributions of sources of systematics listed above to uncertainties in parameters determined from fits to the  $\Upsilon(2S)\pi^+\pi^-$  and  $\Upsilon(3S)\pi^+\pi^-$  data are more uniform. All the contributions are added in quadrature to obtain the overall systematic uncertainty.

## VI. CONCLUSIONS

In conclusion, we have performed a full amplitude analysis of three-body  $e^+e^- \rightarrow \Upsilon(nS)\pi^+\pi^-$  ( $n = 1, 2, 3$ ) transitions that allowed us to determine the relative

fractions of various quasi-two-body components of the three-body amplitudes as well as the spin and parity of the two observed  $Z_b$  states. The favored quantum numbers are  $J^P = 1^+$  for both  $Z_b$  states, while the alternative  $J^P = 1^-$  and  $J^P = 2^\pm$  combinations are rejected at confidence levels exceeding 6 standard deviations. This is a substantial improvement over the previous one-dimensional angular analysis reported in Ref. [5]. This is due to the fact that the part of the amplitude most sensitive to the spin and parity of the  $Z_b$  states is the interference term between the  $Z_b\pi$  and the nonresonant amplitudes. Thus, the highest sensitivity is provided by the  $e^+e^- \rightarrow \Upsilon(2S)\pi^+\pi^-$  transition, where the two amplitudes  $Z_b\pi$  and the nonresonant one are comparable in size. The measured values of the spin and parity of the  $Z_b$  states are in agreement with the expectations of the molecular model [21] yet do not contradict several alternative interpretations [22].

We update the measurement of the three-body  $e^+e^- \rightarrow \Upsilon(nS)\pi^+\pi^-$  cross sections with significantly increased integrated luminosity compared to that in Ref. [1]. The results reported here supersede our measurements reported in Ref. [1]. We also report the first measurement of the relative fractions of the  $e^+e^- \rightarrow Z_b^\mp \pi^\pm$  transitions and the first observation of the  $e^+e^- \rightarrow \Upsilon(1S)f_0(980)$  transition. Finally, we find a significant contribution from the  $e^+e^- \rightarrow \Upsilon(1S)(\pi^+\pi^-)_{D\text{-wave}}$  amplitude but cannot attribute it unambiguously to the  $\Upsilon(1S)f_2(1270)$  channel: the data can be equally well described by adding a  $D$ -wave component to the nonresonant amplitude.

## ACKNOWLEDGEMENT

We thank the KEKB group for the excellent operation of the accelerator; the KEK cryogenics group for the efficient operation of the solenoid; and the KEK computer group, the National Institute of Informatics, and the PNNL/EMSL computing group for valuable computing and SINET4 network support. We acknowledge support from the Ministry of Education, Culture, Sports, Science, and Technology (MEXT) of Japan, the Japan Society for the Promotion of Science (JSPS), and the Tau-Lepton Physics Research Center of Nagoya University; the Australian Research Council and the Australian Department of Industry, Innovation, Science and Research; Austrian Science Fund under Grant No. P 22742-N16; the National Natural Science Foundation of China under Contracts No. 10575109, No. 10775142, No. 10825524, No. 10875115, No. 10935008 and No. 11175187; the Ministry of Education, Youth and Sports of the Czech Republic under Contract No. LG14034; the Carl Zeiss Foundation, the Deutsche Forschungsgemeinschaft and the VolkswagenStiftung; the Department of Science and Technology of India; the Istituto Nazionale di Fisica Nucleare of Italy; the WCU program of the Ministry Education Science and Technology, National Research

Foundation of Korea Grants No. 2011-0029457, No. 2012-0008143, No. 2012R1A1A2008330, and No. 2013R1A1A3007772; the BRL program under NRF Grant No. KRF-2011-0020333 and No. KRF-2011-0021196, Center for Korean J-PARC Users, No. NRF-2013K1A3A7A06056592; the BK21 Plus program and the GSDC of the Korea Institute of Science and Technology Information; the Polish Ministry of Science and Higher Education and the National Science Center; the Ministry of Education and Science of the Russian Federation, the Russian Federal Agency for Atomic Energy and the Russian Foundation for Basic Research Grants No. RFBR 12-02-01296 and No. 12-02-33015; the Slovenian Research Agency; the Basque Foundation for Science (IKERBASQUE) and the UPV/EHU under program UFI 11/55; the Swiss National Science Foundation; the National Science Council and the Ministry of Education of Taiwan; and the U.S. Department of Energy and the National Science Foundation. This work is supported by a Grant-in-Aid from MEXT for Science Research in a Priority Area (“New Development of Flavor Physics”) and from JSPS for Creative Scientific Research (“Evolution of Tau-lepton Physics”).

#### APPENDIX: THE $e^+e^- \rightarrow \Upsilon(nS)\pi^+\pi^-$ AMPLITUDE

Here, we present a Lorentz invariant form of the amplitude for the  $e^+e^- \rightarrow [\Upsilon(nS)\pi_2]\pi_1$ ,  $\Upsilon(nS) \rightarrow \mu^+\mu^-$  transition. The amplitude might consist of several components, each describing a quasi-two-body process with a certain spin and parity of the intermediate state. The following symbols are used:  $P_+$ ,  $P_-$ ,  $K_1$ ,  $K_2$ ,  $P_1$  and  $P_2$  are 4-momenta for the initial state  $e^+$ ,  $e^-$ , and final state  $\mu^+$ ,  $\mu^-$ ,  $\pi_1$  and  $\pi_2$ , respectively;  $Q_0 = P_1 + P_2$ ;  $Q_1 = Q_2 + P_2$ ;  $Q_2 = K_1 + K_2$ ;  $P_0 = Q_1 + P_1$ ; and  $\varepsilon_5$  and  $\varepsilon_n$  are polarization vectors for the virtual photon and  $\Upsilon(nS)$ , ( $n = 1, 2, 3$ ), respectively. Greek indices denote 4-momenta components and run from 0 to 3. The  $e^+e^- \rightarrow \Upsilon(nS)\pi^+\pi^-$  amplitude can be written as

$$\begin{aligned} \mathcal{M}_{\Upsilon(nS)\pi\pi} &= \mathcal{M}_{e^+e^- \rightarrow \Upsilon(nS)\pi^+\pi^-} \mathcal{M}_{\Upsilon(nS) \rightarrow \mu^+\mu^-} \\ &= \varepsilon_5^\mu O_{\mu\nu} \varepsilon_n^{*\nu} \varepsilon_n^\alpha (\bar{u}_1 \gamma_\alpha u_2) \end{aligned} \quad (\text{A1})$$

and

$$|\mathcal{M}_{\Upsilon(nS)\pi\pi}|^2 = \varepsilon_5^{\mu'} \varepsilon_5^\mu O_{\mu\nu} \varepsilon_n^{*\nu} \varepsilon_n^\alpha \text{Sp}(K_1 \gamma_\alpha K_2 \gamma_{\alpha'}) \varepsilon_n^{*\alpha'} \varepsilon_n^{\nu'} O_{\mu'\nu'}^* \quad (\text{A2})$$

where  $u_k$  are the muon spinors. Performing the summation over the repetitive Greek indices and neglecting the muon mass, one obtains

$$\begin{aligned} R^{\nu\nu'} &= \varepsilon_n^{*\nu} \varepsilon_n^\alpha \text{Sp}(K_1 \gamma_\alpha K_2 \gamma_{\alpha'}) \varepsilon_n^{*\alpha'} \varepsilon_n^{\nu'} \\ &= 4(K_1^\nu K_2^{\nu'} + K_2^\nu K_1^{\nu'} - g^{\nu\nu'} (K_1 \cdot K_2)), \end{aligned} \quad (\text{A3})$$

where  $(K_1 \cdot K_2) = g_{\mu\nu} K_1^\mu K_2^\nu$ , and we used  $\varepsilon_n^{*\nu} \varepsilon_n^{\alpha} = g^{\nu\alpha} - \frac{Q_2^\nu Q_2^\alpha}{Q_2^2}$ . Thus, we arrive at

$$|\mathcal{M}_{\Upsilon(nS)\pi\pi}|^2 = \delta_\perp^{\mu\mu'} O_{\mu\nu} R^{\nu\nu'} O_{\nu'\mu'}^*, \quad (\text{A4})$$

where, neglecting the electron mass,

$$\delta_\perp^{\mu\nu} = \frac{(P_+^\mu P_-^\nu + P_-^\mu P_+^\nu)}{(P_+ \cdot P_-)} - g^{\mu\nu} \quad (\text{A5})$$

which is in the c.m. frame with the  $z$ -axis along the  $e^-$  momentum  $\delta_\perp^{\mu\nu} = 1$  if  $\mu = \nu = 1, 2$  and  $\delta_\perp^{\mu\nu} = 0$  otherwise. The factor  $O_{\mu\nu}$  depends on the dynamics of the  $e^+e^- \rightarrow \Upsilon(nS)\pi_1\pi_2$  process (see below). In what follows, we consider only the following possible contributions to the three-body amplitude:  $e^+e^- \rightarrow Z_b\pi_1$ ,  $Z_b \rightarrow \Upsilon(nS)\pi_2$  and  $e^+e^- \rightarrow \Upsilon(nS)(\pi_1\pi_2)_{S,D}$ , where  $(\pi_1\pi_2)_{S,D}$  denotes the system of two pions in an  $S$ - and  $D$ -wave configuration, respectively. We consider the following combinations of spin and parity of the intermediate  $Z_b$  state:  $J_{Z_b}^P = 1^+, 1^-, 2^+$  and  $2^-$ . Factors  $O_{\mu\nu}$  corresponding to these six amplitudes are given below.

- (1)  $J_{Z_b}^P = 1^-$ . Although both  $P$ - and  $F$ -waves are allowed for the  $\pi_2$  here (and in the case of  $J_{Z_b}^P = 2^-$ ), the  $F$ -wave is substantially suppressed by the phase space factor, so we keep only the  $P$ -wave component of the amplitude

$$\begin{aligned} O_{\Upsilon\pi_2}^{\mu\nu} &= \varepsilon_\alpha^* \varepsilon^{\mu\alpha\rho} P_{0\gamma} Q_{1\rho} \varepsilon_\sigma \varepsilon^{\nu\sigma\delta\kappa} Q_{1\delta} Q_{2\kappa} \\ &= g^{\mu\nu} ((P_0 \cdot Q_1)(Q_1 \cdot Q_2) - (P_0 \cdot Q_2)Q_1^2) \\ &\quad + Q_2^\mu P_0^\nu Q_1^2 - Q_2^\mu Q_1^\nu (P_0 \cdot Q_1) \\ &\quad + Q_1^\mu Q_1^\nu (P_0 \cdot Q_2) - Q_1^\mu P_0^\nu (Q_1 \cdot Q_2). \end{aligned} \quad (\text{A6})$$

- (2)  $J_{Z_b}^P = 1^+$ . In this case (as well as in the case of  $J_{Z_b}^P = 2^+$ )  $S$ - and  $D$ -waves are allowed for the  $\pi_2$ . We keep only the  $S$ -wave since the  $D$ -wave is suppressed by the phase space factor. Thus

$$\begin{aligned} O_{\Upsilon\pi_2}^{\mu\nu} &= (g^{\mu\alpha} + a_1 P_1^\mu P_1^\alpha) \varepsilon_\alpha^* \varepsilon_\beta (g^{\mu\beta} + a_2 P_2^\beta P_2^\nu) \\ &= g^{\mu\nu} + a_1 P_1^\mu P_1^\nu + a_2 P_2^\mu P_2^\nu \\ &\quad - \frac{Q_1^\mu Q_1^\nu}{Q_1^2} (1 - a_1(Q_1 \cdot P_1) + a_2(Q_1 \cdot P_2)) \\ &\quad + a_0 a_1 a_2 P_1^\mu P_2^\nu, \end{aligned} \quad (\text{A7})$$

where

$$\begin{aligned}
a_0 &= (P_1 \cdot P_2) - \frac{(Q_1 \cdot P_1)(Q_1 \cdot P_2)}{Q_1^2}; \\
a_1 &= \frac{(P_0 \cdot Q_1) - \sqrt{P_0^2 Q_1^2}}{(Q_1 \cdot P_1)^2 - m_\pi^2 Q_1^2}; \\
a_2 &= \frac{(Q_1 \cdot Q_2) - \sqrt{Q_1^2 Q_2^2}}{(Q_2 \cdot P_2)^2 - m_\pi^2 Q_2^2}, \quad (\text{A8})
\end{aligned}$$

$$\text{and } \varepsilon_\alpha^* \varepsilon_\beta = (g_{\alpha\beta} - \frac{Q_{1\alpha} Q_{1\beta}}{Q_1^2}).$$

$$(3) J_{Z_b}^P = 2^-.$$

$$O_{\Upsilon\pi_2}^{\mu\nu} = \varepsilon_{\alpha\beta}^* \varepsilon^{\mu\alpha\gamma\rho} P_{0\gamma} Q_{1\rho} P_0^\beta \varepsilon_{\sigma\tau} \varepsilon^{\nu\sigma\delta\kappa} Q_{1\delta} Q_{2\kappa} Q_2^\tau. \quad (\text{A9})$$

Taking into account that

$$\varepsilon_{\alpha\beta}^* \varepsilon_{\sigma\delta} = \frac{1}{2} (G_{\alpha\sigma} G_{\beta\delta} + G_{\alpha\delta} G_{\beta\sigma}) - \frac{1}{3} G_{\alpha\beta} G_{\sigma\delta}, \quad (\text{A10})$$

where  $G_{\alpha\beta} = g_{\alpha\beta} - \frac{Q_{1\alpha} Q_{1\beta}}{Q_1^2}$ , we obtain

$$\begin{aligned}
O_{\Upsilon\pi_2}^{\mu\nu} &= \frac{1}{2} \left[ (g^{\mu\nu} [(P_0 \cdot Q_1)(Q_1 \cdot Q_2) - (P_0 \cdot Q_2) Q_1^2] \right. \\
&\quad + Q_2^\mu P_0^\nu Q_1^2 - Q_2^\mu Q_1^\nu (P_0 \cdot Q_1) \\
&\quad + Q_1^\mu Q_2^\nu (P_0 \cdot Q_2) - Q_1^\mu P_0^\nu (Q_1 \cdot Q_2)) \\
&\quad \left. \times \left( (P_0 \cdot Q_2) - \frac{(P_0 \cdot Q_1)(Q_1 \cdot Q_2)}{Q_1^2} \right) - d^\mu d^\nu \right], \quad (\text{A11})
\end{aligned}$$

where  $d^\mu = \varepsilon_{\nu\alpha\beta}^\mu P_0^\nu Q_1^\alpha Q_2^\beta$  and  $\varepsilon_{\nu\alpha\beta}^\mu = g^{\mu\sigma} \varepsilon_{\sigma\nu\alpha\beta}$  and  $\varepsilon_{\sigma\nu\alpha\beta}$  is an antisymmetric tensor.

$$(4) J_{Z_b}^P = 2^+.$$

$$O_{\Upsilon\pi_2}^{\mu\nu} = \varepsilon_{\kappa\sigma}^* (g^{\mu\kappa} + a_1 P_1^\mu P_1^\kappa) P_1^\sigma \varepsilon_{\alpha\beta} (g^{\alpha\nu} + a_2 P_2^\alpha P_2^\nu) P_2^\beta$$

and

$$\begin{aligned}
O_{\Upsilon\pi_2}^{\mu\nu} &= g^{\mu\nu} \frac{a_0}{2} + \frac{P_2^\mu P_1^\nu}{2} + P_2^\mu P_2^\nu \left( a_0 a_2 - \frac{(Q_1 \cdot P_1)}{2Q_1^2} \right) + P_1^\mu P_1^\nu \left( a_0 a_1 - \frac{(Q_1 \cdot P_2)}{2Q_1^2} \right) \\
&\quad + \frac{1}{3} \frac{Q_1^\mu Q_1^\nu}{Q_1^4} \left[ (P_0 \cdot Q_1)(Q_1 \cdot Q_2) + 3(Q_1 \cdot P_1)(Q_1 \cdot P_2) - \frac{3}{2} (P_1 \cdot P_2) Q_1^2 + a_2 ((P_0 \cdot Q_1)(m_\pi^2 Q_1^2 - (Q_1 \cdot P_2)^2)) \right. \\
&\quad + a_1 ((Q_1 \cdot Q_2)(m_\pi^2 Q_1^2 - (Q_1 \cdot P_1)^2)) + 3a_0 Q_1^2 (a_1 (Q_1 \cdot P_1) - a_2 (Q_1 \cdot P_2)) \\
&\quad \left. - a_1 a_2 (3a_0^2 Q_1^4 - (m_\pi^2 Q_1^2 - (Q_1 \cdot P_1)^2)(m_\pi^2 Q_1^2 - (Q_1 \cdot P_2)^2)) \right], \quad (\text{A12})
\end{aligned}$$

where factors  $a_0$ ,  $a_1$ , and  $a_2$  are the same as in Eq. (A7).

In the case of production of the  $\pi^+\pi^-$  system with defined spin and parity, we assume that spin structure of the  $b\bar{b}$  pair is not modified and the  $\pi^+\pi^-$  system is produced in an  $S$ -wave with respect to the  $\Upsilon(nS)$  state and decays depending on its spin. We consider two cases: the relative angular momentum of the two pions being equal to zero (decay in an  $S$ -wave) and equal to two (decay in a  $D$ -wave).

The  $O^{\mu\nu}$  factor for these parts of the three-body  $e^+e^- \rightarrow \Upsilon(nS)\pi^+\pi^-$  amplitude can be written as follows.

(5)  $S$ -wave.

$$O_S^{\mu\nu} = g^{\mu\nu} + Q_0^\mu Q_0^\nu \frac{(P_0 \cdot Q_2) - \sqrt{P_0^2 Q_2^2}}{(Q_0 \cdot Q_2)^2 - Q_0^2 Q_2^2}. \quad (\text{A13})$$

(6)  $D$ -wave.

$$O_D^{\mu\nu} = O_S^{\mu\nu} \left[ (P_0 \cdot P_1)^2 - \frac{2(P_0 \cdot P_1)(Q_0 \cdot P_1)(P_0 \cdot Q_0)}{Q_0^2} + \frac{(P_0 \cdot Q_0)^2 (Q_0 \cdot P_1)^2}{Q_0^4} - \frac{1}{3} \left( P_0^2 - \frac{(P_0 \cdot Q_0)}{Q_0^2} \right) \left( m_\pi^2 - \frac{(Q_0 \cdot P_1)^2}{Q_0^2} \right) \right]. \quad (\text{A14})$$

The combined  $O^{\mu\nu}$  in Eq. (A4) is then calculated as

$$O^{\mu\nu} = a_S(s_{23}) O_S^{\mu\nu} + a_D(s_{23}) O_D^{\mu\nu} + c_{Z_1} e^{i\delta_{Z_1}} (a_{Z_1}(s_{12}) O_{\Upsilon\pi_1}^{\mu\nu} + a_{Z_1}(s_{13}) O_{\Upsilon\pi_2}^{\mu\nu}) + c_{Z_2} e^{i\delta_{Z_2}} (a_{Z_2}(s_{12}) O_{\Upsilon\pi_1}^{\mu\nu} + a_{Z_2}(s_{13}) O_{\Upsilon\pi_2}^{\mu\nu}), \quad (\text{A15})$$



where  $s_{12} = M^2(\Upsilon(nS)\pi_1)$ ,  $s_{13} = M^2(\Upsilon(nS)\pi_2)$ , and  $s_{23} = M^2(\pi^+\pi^-)$  ( $s_{23}$  can be expressed via  $s_{12}$  and  $s_{13}$  but we prefer to keep it here for clarity);  $c_{Z_k}$  and  $\delta_{z_k}$  are free parameters of the fit. Note that the  $Z_k$  amplitudes in Eq. (A15) are symmetrized with respect to  $\pi_1$  and  $\pi_2$  interchange to obey isospin symmetry.

In this analysis, the  $S$ -wave part of the amplitude is comprised of the following possible modes:  $\Upsilon(nS)\sigma(500)$ ,  $\Upsilon(nS)f_0(980)$  and a nonresonant one, that is,

$$a_S(s_{23}) = c_\sigma e^{i\delta_\sigma} a_\sigma(s_{23}) + c_{f_0} e^{i\delta_{f_0}} a_{f_0}(s_{23}) + \mathcal{A}^{\text{NR}}(s_{23}), \quad (\text{A16})$$

where  $a_\sigma(s_{23})$  is a Breit-Wigner function and  $a_{f_0}(s_{23})$  is parametrized by a Flatté function. Following the suggestion given in Refs. [23,24], the nonresonant amplitude  $\mathcal{A}^{\text{NR}}(s_{23})$  is parametrized as

$$\mathcal{A}^{\text{NR}}(s_{23}) = c_1^{\text{NR}} e^{i\delta_1^{\text{NR}}} + c_2^{\text{NR}} e^{i\delta_2^{\text{NR}}} s_{23}. \quad (\text{A17})$$

The  $D$ -wave part of the three-body amplitude consists of only the  $\Upsilon(nS)f_2(1270)$  mode

$$a_D(s_{23}) = c_{f_2} e^{i\delta_{f_2}} a_{f_2}(s_{23}), \quad (\text{A18})$$

where  $a_{f_2}(s_{23})$  is a Breit-Wigner function with the mass and width fixed at world average values [13]. In the study of a model-related uncertainty, we also fit the data with  $a_{f_2}(s_{23})$  replaced by just an  $s_{23}$  term to represent a possible  $D$ -wave component of the nonresonant amplitude. Parameters  $c_X$ ,  $c_k^{\text{NR}}$ , and phases  $\delta_X$  and  $\delta_k^{\text{NR}}$  in Eqs. (A16)–(A18) are free parameters of the fit. Finally, terms  $a_{Z_k}(s)$  in Eq. (A15) are parametrized by Breit-Wigner functions with masses and widths to be determined from the fit.

Since we are sensitive to the relative phases and amplitudes only, we are free to fix one phase and one amplitude in Eq. (A15). In the analysis of the  $\Upsilon(1S)\pi^+\pi^-$  mode, we fix  $c_1^{\text{NR}} = 1$  and  $\delta_1^{\text{NR}} = 0$ ; in the analysis of the  $\Upsilon(2S)\pi^+\pi^-$  and  $\Upsilon(3S)\pi^+\pi^-$  modes, we fix the amplitude and the phase of the  $Z_b(10610)$  component to  $c_{Z_1} = 1$  and  $\delta_{Z_1} = 0$ .

- 
- [1] K. F. Chen *et al.* (Belle Collaboration), *Phys. Rev. Lett.* **100**, 112001 (2008).
- [2] I. Adachi *et al.* (Belle Collaboration), *Phys. Rev. Lett.* **108**, 032001 (2012).
- [3] A. Bondar *et al.* (Belle Collaboration), *Phys. Rev. Lett.* **108**, 122001 (2012).
- [4] P. Krokovny *et al.* (Belle Collaboration), *Phys. Rev. D* **88**, 052016 (2013).
- [5] I. Adachi *et al.* (Belle Collaboration), arXiv:1105.4583.
- [6] S. Kurokawa and E. Kikutani, *Nucl. Instrum. Methods Phys. Res., Sect. A* **499**, 1 (2003), and other papers included in this Volume; T. Abe *et al.* *Prog. Theor. Exp. Phys.* **2013**, 03A001 (2013) and following articles up to 03A011
- [7] A. Abashian *et al.* (Belle Collaboration), *Nucl. Instrum. Methods Phys. Res., Sect. A* **479**, 117 (2002); also see detector section in J. Brodzicka *et al.*, *Prog. Theor. Exp. Phys.* **2012**, 04D001 (2012).
- [8] D. J. Lange, *Nucl. Instrum. Methods Phys. Res., Sect. A* **462**, 152 (2001).
- [9] E. Barberio and Z. Was, *Comput. Phys. Commun.* **79**, 291 (1994).
- [10] R. Brun *et al.*, GEANT 3.21, CERN Report No. DD/EE/84-1, 1984.
- [11] J. E. Gaiser, Ph.D. thesis, SLAC-R-255, 1982 (unpublished); T. Skwarnicki, Ph.D. thesis, DESY F31-86-02, 1986 (unpublished).
- [12] A. Garmash *et al.* (Belle Collaboration), *Phys. Rev. Lett.* **96**, 251803 (2006).
- [13] J. Beringer *et al.* (Particle Data Group), *Phys. Rev. D* **86**, 010001 (2012).
- [14] A. Garmash *et al.* (Belle Collaboration), *Phys. Rev. D* **71**, 092003 (2005).
- [15] M. Williams, *JINST* **5**, P09004 (2010) and references therein.
- [16] M. G. Kendall and A. Stuart, *The Advanced Theory of Statistics*, 2nd ed. (Hafner Publishing, New York, 1968).
- [17] E. A. Kuraev and V. S. Fadin, *Sov. J. Nucl. Phys.* **41**, 466 (1985); M. Benayoun, S. I. Eidelman, V. N. Ivanchenko, and Z. K. Silagadze, *Mod. Phys. Lett. A* **14**, 2605 (1999).
- [18] D. Santel *et al.* (Belle Collaboration), arXiv:1501.01702.
- [19] S. Actis *et al.*, *Eur. Phys. J. C* **66**, 585 (2010).
- [20] S. Esen *et al.* (Belle Collaboration), *Phys. Rev. D* **87**, 031101(R) (2013).
- [21] A. E. Bondar, A. Garmash, A. I. Milstein, R. Mizuk, and M. B. Voloshin, *Phys. Rev. D* **84**, 054010 (2011).
- [22] D.-Y. Chen and X. Liu, *Phys. Rev. D* **84**, 094003 (2011); A. Ali, C. Hambrock, and W. Wang, *Phys. Rev. D* **85**, 054011 (2012); I. V. Danilkin, V. D. Orlovsky, and Y. A. Simonov, *Phys. Rev. D* **85**, 034012 (2012); S. Ohkoda, Y. Yamaguchi, S. Yasui, K. Sudoh, and A. Hosaka, *Phys. Rev. D* **86**, 014004 (2012); E. Braaten, C. Langmack, and D. Hudson Smith, *Phys. Rev. D* **90**, 014044 (2014).
- [23] M. B. Voloshin, *Prog. Part. Nucl. Phys.* **61**, 455 (2008).
- [24] M. B. Voloshin, *Phys. Rev. D* **74**, 054022 (2006).